



**HAL**  
open science

## Recent and historical pollution legacy in high altitude Lake Marboré (Central Pyrenees): A record of mining and smelting since pre-Roman times in the Iberian Peninsula

J.P. Corella, M.J. Sierra, A. Garralón, R. Millan, J. Rodríguez-Alonso, M.P. Mata, A. Vicente de Vera, A. Moreno, P. González-Sampériz, B. Duval, et al.

### ► To cite this version:

J.P. Corella, M.J. Sierra, A. Garralón, R. Millan, J. Rodríguez-Alonso, et al.. Recent and historical pollution legacy in high altitude Lake Marboré (Central Pyrenees): A record of mining and smelting since pre-Roman times in the Iberian Peninsula. *Science of the Total Environment*, 2021, 751, pp.141557. 10.1016/j.scitotenv.2020.141557 . hal-02931525

**HAL Id: hal-02931525**

**<https://hal.science/hal-02931525v1>**

Submitted on 1 Feb 2022

**HAL** is a multi-disciplinary open access archive for the deposit and dissemination of scientific research documents, whether they are published or not. The documents may come from teaching and research institutions in France or abroad, or from public or private research centers.

L'archive ouverte pluridisciplinaire **HAL**, est destinée au dépôt et à la diffusion de documents scientifiques de niveau recherche, publiés ou non, émanant des établissements d'enseignement et de recherche français ou étrangers, des laboratoires publics ou privés.

1        **Recent and historical pollution legacy in high altitude Lake**  
2        **Marboré (Central Pyrenees): a record of mining and smelting**  
3        **since pre-Roman times in the Iberian Peninsula**

4

5        J.P. Corella<sup>1\*</sup>, M.J. Sierra<sup>2</sup>, A. Garralón<sup>2</sup>, R. Millán<sup>2</sup>, J. Rodríguez-Alonso<sup>2</sup>, M.P. Mata<sup>3</sup>,  
6        A. Vicente de Vera<sup>4</sup>, A. Moreno<sup>4</sup>, P. González-Sampériz<sup>4</sup>, B Duval<sup>5</sup>, D. Amouroux<sup>5</sup>, P.  
7        Vivez<sup>6</sup>, C.A. Cuevas<sup>7</sup>, J.A Adame<sup>8</sup>, B. Wilhelm<sup>1</sup>, A. Saiz-Lopez<sup>7</sup>, B.L. Valero- Garcés<sup>4</sup>

8

9        <sup>1</sup>Universite Grenoble Alpes, CNRS, IRD, IGE, 38000 Grenoble, France.

10       <sup>2</sup>CIEMAT — Environmental Department (DMA), Avenida Complutense 40, E-28040 Madrid, Spain.

11       <sup>3</sup>Instituto Geológico y Minero de España, Rios Rosas 23, 28003 Madrid, Spain.

12       <sup>4</sup>Pyrenean Institute of Ecology, CSIC, Avda Montañana 1005, 50059 Zaragoza, Spain.

13       <sup>5</sup>Universite de Pau et des Pays de l'Adour, E2S UPPA, CNRS, IPREM, Institut des Sciences Analytiques et de  
14       Physico-chimie pour l'Environnement et les matériaux, Pau, France, 64000 Pau, France.

15       <sup>6</sup>Centro de Estudios de Sobrarbe, Sociedad Española para la Defensa del Patrimonio Geológico Y Minero, Plaza  
16       España, 22340 Boltaña, Huesca, Spain.

17       <sup>7</sup>Department of Atmospheric Chemistry and Climate, Institute of Physical Chemistry Rocasolano, CSIC, Serrano 119,  
18       28006 Madrid, Spain.

19       <sup>8</sup>Atmospheric Sounding Station, El Arenosillo Observatory, Atmospheric Research and Instrumentation Branch,  
20       National Institute for Aerospace Technology (INTA), Mazagón, Huelva, Spain..

21       \*Corresponding author: pcorella@iqfr.csic.es

22

23       **ABSTRACT**

24

25       We have analysed potential harmful trace elements (PHTE; Pb, Hg, Zn, As and Cu) on  
26       sediment cores retrieved from lake Marboré (LM) (2612 m a.s.l, 42°41'N; 0° 2'E).

27       PHTE variability allowed us to reconstruct the timing and magnitude of trace metal

28 pollutants fluxes over the last 3000 years in the Central Pyrenees. A statistical treatment  
29 of the dataset (PCA) enabled us to discern the depositional processes of PHTE, that  
30 reach the lake via direct atmospheric deposition. Indeed, the location of LM above the  
31 atmospheric boundary layer makes this lake an exceptional site to record the long-range  
32 transport of atmospheric pollutants in the free troposphere. Air masses back-trajectories  
33 analyses enabled us to understand the transport pathways of atmospheric pollutants  
34 while lead isotopic analyses contributed to evaluate the source areas of metal pollution  
35 in SW Europe during the Late Holocene. PHTE variability, shows a clear agreement  
36 with the main exploitation phases of metal resources in Southern Europe during the Pre-  
37 Industrial Period. We observed an abrupt lead enrichment from 20 to 375 yrs CE mostly  
38 associated to silver and lead mining and smelting practices in Southern Iberia during the  
39 Roman Empire. This geochemical data suggests that regional atmospheric metal  
40 pollution during the Roman times rivalled the Industrial Period. PHTE also increased  
41 during the High and Late Middle Ages (10-15<sup>th</sup> centuries) associated to a reactivation of  
42 mining and metallurgy activities in high altitude Pyrenean mining sites during climate  
43 amelioration phases. Atmospheric mercury deposition in the Lake Marboré record  
44 mostly reflects global emissions, particularly from Almadén mines (central Spain) and  
45 slightly fluctuates during the last three millennia with a significant increase during the  
46 last five centuries. Our findings reveal a strong mining-related pollution legacy in alpine  
47 lakes and watersheds that needs to be considered in management plans for mountain  
48 ecosystems as global warming and human pressure effects may contribute to their future  
49 degradation.

50 **KEY WORDS:** Atmospheric pollution, lakes, trace metals, historical mining, Pyrenees

51

## 52        **1- INTRODUCTION**

53 Metallurgy has been key for the development of human society during Pre-industrial  
54 times (Killick and Fenn, 2012). The Iberian Peninsula is particularly rich in mineral  
55 resources and has a long history of mining and smelting activities with several of the  
56 world's most representative historical mining districts. Almadén mines, located in  
57 Central Spain, has been the World's largest mercury (Hg) mine until its closure at the  
58 turn of this century. This mine has been actively exploited during two millennia  
59 producing 30 % of the globally mined Hg with an accumulated historic Hg emission  
60 estimate of 10 000 tons (Hylander and Meili, 2003). Southern Iberia is also very rich in  
61 mineral resources hosting important silver (Ag) and lead (Pb) mining hotspots. These  
62 resources have been exploited for several millennia, with more than 10 000 tons of Pb  
63 produced contributing to 40 % of the World's total lead production between 1200 BCE  
64 (before Common Era) and 500 CE (Common Era). Most of the Iberian Ag and Pb  
65 mining located in Rio Tinto and Mazarrón-Cartagena mining districts were intensively  
66 exploited by Phoenicians, Carthaginians and Romans.

67        In NW Iberia, mining and metallurgy started in the Chalcolithic–Early Bronze  
68 Age 4500 years ago according to archaeological information (de Blas, 1996, 2005)  
69 although the first atmospheric pollution signal related to these human activities has been  
70 dated 500 years before (~5 kyrs ago) (Martínez-Cortizas et al., 2016). To a lesser extent,  
71 the Pyrenees has also been largely exploited during the last centuries for Ag and Pb  
72 production (e.g. Ariturri mines in Western Pyrenees (Thalacker, 1804), Emporion  
73 mines in Catalonia (Montero-Ruiz et al., 2007)). Southern Central Pyrenees also have  
74 local rich deposits of metals including copper (Cu), Pb, Ag and iron (Fe), many of them  
75 historically mined and processed at high elevation emplacements (>2000 m a.s.l.) (e.g.

76 Bielsa-Parzán mining district (Calvo, 2008; Nieto-Callen, 1996)), although the timeline  
77 of their activities is not well constrain prior to the last 500 years.

78           Unfortunately, historical mining and metalworking activities have left a long-  
79 lasting imprint on the environment (Hansson et al., 2019). Indeed, although numerous  
80 natural and anthropogenic activities can increase contaminant levels in the environment,  
81 mining operations are notable regarding the number of particulates generated, the global  
82 impact, and the trace metals' toxicity associated with atmospheric pollutant emissions  
83 (Csavina et al., 2012). Thus, large quantities of PHTE such as Pb, Hg, Cu, zinc (Zn) or  
84 arsenic (As) have been released to the regional atmosphere during the last millennia and  
85 subsequently deposited and stored in the Iberian Peninsula (Gallego et al., 2019;  
86 Hanebuth et al., 2018; Kylander et al., 2005; Leblanc et al., 2000; Manteca et al., 2017;  
87 Martínez-Cortizas et al., 1999; 2002; 2012; 2013; 2016; Mil-Homens et al., 2017;  
88 Serrano et al., 2013) among others, and elsewhere in the Northern Hemisphere even in  
89 remote, pristine glacier ice in the Alps and the Arctic (Hong et al., 1994, 1996;  
90 McConnell et al., 2018; 2019; Preunkert et al., 2019; Rosman et al., 1997), regions  
91 located far away from the pollution source. Understanding this environmental legacy,  
92 i.e. the persistence of PHTE pollution overtime from past anthropogenic emissions, and  
93 the fluxes from terrestrial to aquatic ecosystems (Bacardit and Camarero, 2010) should  
94 help environmental policy makers to design future and sustainable environmental  
95 management plans and monitoring programs. Indeed, as recently highlighted by  
96 Camarero (2017) and Le Roux et al. (2019), the long-term PHTE monitoring provided  
97 by natural archives is particularly needed in mountain environments such as the  
98 Pyrenees in order to assess the response of mountain critical zones to Global Change

99           Among natural archives, lake sediments have been widely used to reconstruct  
100 past mining and metalworking activities as well as other anthropogenic sources, e.g.  
101 (Cooke et al., 2011, 2020; Díez et al., 2017; Elbaz-Poulichet et al., 2020; Mariet et al.,  
102 2018; Renberg et al., 1994; Thevenon et al., 2011; Wilhelm et al., 2017). These  
103 continuous sedimentary records allow us to understand the variability of different  
104 mining-related pollution sources through time as well as to assess their environmental  
105 legacy. Surprisingly, yet relatively few pollution records from lacustrine sediments exist  
106 in the Iberian Peninsula (Camarero, 2017; Camarero et al., 1998; Corella et al., 2017;  
107 2018; García-Alix et al., 2013; Hillman et al., 2017; Martín-Puertas et al., 2010). High-  
108 altitude mountain lakes record most efficiently past atmospheric pollution phases due to  
109 enhanced atmospheric precipitation and the “cold trapping” effect caused by elevation  
110 making these locations regional convergence areas of atmospheric pollutants  
111 (Camarero, 2017). Recent depositional patterns based on lake surface sediments show a  
112 W-E distribution with higher trace metal concentrations in the eastern Pyrenees lakes  
113 (Bacardit and Camarero, 2009; Camarero, 2003, 2017). Inventories of trace metals in  
114 soils and sediments in several lake catchments in the central Pyrenees have shown a  
115 large anthropogenic component (Bacardit and Camarero, 2010; Bacardit et al., 2012).  
116 High levels of pre-industrial pollutants have been reported in several Pyrenean lakes  
117 (Camarero et al., 1998; Lavilla et al., 2006), but millennial- long, well-dated records are  
118 scarce (Hansson et al., 2017). Recent research in several well-dated records from  
119 mountain lakes across an altitudinal transect in the Southern Central Pyrenees (NE  
120 Spain) assessed the variable pollutant loading in these ecosystems during the Industrial  
121 period (Corella et al., 2018). This study highlighted that among all studied lakes, high-  
122 altitude, pristine Lake Marboré (LM), located at the Pyrenean summit (> 2600 m. a.s.l.)  
123 records most efficiently past regional atmospheric deposition of PTHE. LM has

124 provided the sedimentary record at the highest altitude in the Pyrenees (Leunda et al.,  
125 2017; Oliva-Urcia et al., 2018) in a privileged location in the free troposphere.  
126 Therefore, LM record can be considered as representative of background, global  
127 atmospheric pollution since long-range transport of atmospheric pollutants mostly takes  
128 place above the atmospheric boundary layer.

129         This study aims to reconstruct the atmospheric pollution in the Pyrenees related  
130 to mining and metalworking activities in the Iberian Peninsula during the main historic  
131 periods of the last three millennia (namely Iron Age (IA; 1000 BCE- 218 BCE), Roman  
132 Period (RP; 218 BCE-476 CE), Early Middle Ages (EMA; 476-1000 CE), High Middle  
133 Ages (HMA; 1000-1300 CE), and Late Middle Ages (LMA; 1300-1492 CE), Modern  
134 Period and beginning of Contemporary Age (MP; 1492-1850 CE) and the Industrial  
135 Period (IP; 1850 CE-Present day). To achieve this goal, we have carried out a multi-  
136 proxy research strategy on the first 175 cm of a sediment core retrieved in the distal are  
137 of LM that comprises the last 3000 years. The multidisciplinary analyses included i) the  
138 determination of major, minor and trace metals that allowed us to quantify the  
139 geochemical composition of the sediments down-core; ii) lead isotopic analyses to  
140 evaluate the possible sources of metal pollution during the different historical phases of  
141 mining production in the Iberian Peninsula, iii) multivariate statistical modelling to  
142 discern the depositional processes of each geochemical element and iv) air masses back-  
143 trajectories computation to evaluate the atmospheric transport pathways of major  
144 pollutants during the last decades.

## 145 **2-STUDY SITE**

146 LM (42°41' N; 0° 2' E, Fig. 1) is a lake emplaced at 2612 m a.s.l. within a glacier cirque  
147 located in the Spanish Central Pyrenees. The lake has a surface area of 14.3 ha and it is

148 emplaced in a watershed of 137 ha (Valero-Garcés et al., 2013), lying on Cretaceous-  
149 Tertiary carbonated rocks (Pujalte et al., 2016; Samsó Escolá and Robador, 2018). Mean  
150 annual temperature and precipitation at the nearest meteorological station (Góriz station,  
151 located at 2220 m a.s.l.) are 4.9°C and ~2000 mm (Leunda et al., 2017). The vegetation  
152 cover around the lake is very scarce with only a few patches of alpine herbs (Leunda et  
153 al., 2017). The lake has a maximum depth of 30 m and an elongated morphology with  
154 ~500 m along the WNW-ESE axis and ~200 m across (Sánchez-España et al., 2018).  
155 Since there is no direct connection with the nearby Monte Perdido and Marboré glaciers  
156 (García-Ruiz et al., 2014), lake level is controlled mostly by precipitation/evaporation  
157 balance (Nicolás-Martínez, 2013; Valero-Garcés et al., 2013) with small ephemeral  
158 inlets and outlets located in the lake's western and southern shores respectively. The  
159 lake was dammed in the 1940s but the dam was never completely functional and it has  
160 been decommissioned. LM is a cold dimictic and ultra-oligotrophic lake which surface  
161 is covered by ice and snow from December to July (Sánchez-España et al., 2018).

162

### 163 **3- MATERIAL AND METHODS**

164 **3.1- Back-trajectories analyses.** To estimate the atmospheric transport pathways to  
165 LM, the back trajectories of air masses were computed using the HYSPLIT (Hybrid  
166 Single-Particle Lagrangian Integrated Trajectory) model developed by NOAA's Air  
167 Resources Laboratory (ARL) (Draxler et al., 2009). The HYSPLIT model is a complete  
168 software for computing simple air parcel trajectories as well as complex transport,  
169 dispersion, chemical transformation, and deposition simulations (Draxler et al., 2009). It  
170 is often used for forward and back-trajectory air masses analysis, and to establish  
171 source-receptor relationships (Stein et al., 2015). The calculation method is a hybrid



172 method between the Lagrangian approach, using a moving frame of reference for  
173 advection and diffusion calculations as the trajectories on air parcels move from their  
174 origin, and the Eulerian methodology using a fixed three-dimensional grid as a frame of  
175 reference to compute pollutant air concentrations (Stein et al., 2015). Three-  
176 dimensional kinematic trajectories were computed daily at 12:00 UTC, with a 72-hour  
177 runtime at 100 m above ground level (agl), taking as arrival point the LM. The back  
178 trajectories were calculated using the meteorological fields of the global meteorological  
179 model ECMWF (European Centre for Medium Range Weather Forecasts). In order to  
180 cover the entire studied period, we used ERA40 and ERA-Interim data reanalysis with  
181 similar spatial and temporal resolutions. The data reanalysis used has a spatial  
182 resolution of  $0.5^\circ$  (latitude x longitude), 22 vertical levels from the surface to 250 mb  
183 and a temporal resolution of 6 h. The back trajectories were calculated every six hours  
184 during the period 1960-2016 CE. Although climate variability has caused changes in  
185 weather conditions and extreme events at local and regional scale and also affected the  
186 intensity of atmospheric circulation dynamics during the Late Holocene (Sánchez-  
187 López et al., 2016), we assumed that general atmospheric circulation patterns has  
188 remained similar, and therefore, that 20-21<sup>st</sup> century air masses back trajectories are  
189 representative of the studied period (i.e. last 3000 years). ERA40 data reanalysis were  
190 used for the computation of back trajectories for the period 1960- 1993 CE, while ERA-  
191 Interim for the period 1994-2016 yrs CE (Dee et al., 2011). These meteorological fields  
192 were converted into the ARL standard format using the HYSPLIT model. Back-  
193 trajectories from 1960 to 2016 yrs CE have been added on a  $0.25^\circ \times 0.25^\circ$  grid to  
194 visualize air masses sources (frequency map shown in Fig 1). Frequency map represents  
195 the number of back-trajectories passing above every location before arriving to LM in  
196 the 1960-2016 yrs CE time period. To estimate the main source areas of these

197 trajectories arriving to LM we have defined several regions and calculated the number  
198 of trajectories passing through those regions before arriving to LM (Table 1). Note that  
199 since back-trajectories pass above more than one region before arriving to LM, the sum  
200 of all percentages does not equal 100%. For calculation of specific emission sources  
201 (i.e. mining districts) we have considered for each site an area equal to its location  $\pm 2^\circ$   
202 (latitude and longitude).

203

204 **3.2- Sediment cores and age-depth model.** A long (~7 m) sediment core (MAR11-  
205 1U) and a short (0,2 m) gravity (MAR11-1G-1U) were retrieved in august 2011 from  
206 the deepest part of LM using an UWITEC floating platform and coring equipment from  
207 the Pyrenean Institute of Ecology (IPE-CSIC) (Oliva-Urcia et al., 2018). Core  
208 correlation between the short and the long core was carried out using the Pb  
209 concentration profiles (Oliva-Urcia et al., 2018). For the development of the composite  
210 UWITEC sedimentary sequence we used consecutive sections since the recovery factor  
211 was excellent. Sediment cores were split lengthwise for sedimentary facies description  
212 and discrete sampling. A continuous sampling was carried out every 2 cm was carried  
213 out for geochemical analyses. LM sediments during the Late Holocene mainly consists  
214 of laminated siliciclastic mud with very low Total Organic Carbon content (TOC  
215 ranging from 0.1 to 1.1%) (Corella et al., 2018; Oliva-Urcia et al., 2018; Valero-Garcés  
216 et al., 2013). Recent sedimentation has been characterized with sediment traps located  
217 in the deeper areas of the lake since 2017. Annual surveys include water sampling and  
218 temperature, pH, conductivity and oxygen depth profiles.

219 The chronology for the Late Holocene sediment sequence in LM was developed  
220 using five Accelerator Mass Spectrometry (AMS)  $^{14}\text{C}$  radiometric dates from long core  
221 MAR11-1U and  $^{137}\text{Cs}/^{210}\text{Pb}$  dating performed from the gravity core MAR11-1G-1U.

222  $^{210}\text{Pb}$  dating in the short core was obtained by gamma ray spectrometry. Excess  
223 (unsupported)  $^{210}\text{Pb}$  was calculated by the difference between total  $^{210}\text{Pb}$  and  $^{214}\text{Pb}$  for  
224 individual core intervals.  $^{210}\text{Pb}$  chronology was determined using the constant rate of  
225 supply (CRS) model (Appleby, 2001). The  $^{210}\text{Pb}$  age model is supported by the presence  
226 of a  $^{137}\text{Cs}$  peak at 6 cm (AD 1963) in agreement with the  $^{210}\text{Pb}$  chronology (Leunda et  
227 al., 2017; Oliva-Urcia et al., 2018). The age-depth model has been constructed by linear  
228 interpolation between the median ages of the probability distribution of adjacent  
229 calibrated dates (see Leunda et al., (2017) and Oliva-Urcia et al., (2018)) for a complete  
230 description and information of the LM age-depth model). In this study we have focused  
231 in the upper 175 cm of the studied sedimentary sequence that comprises the period 1032  
232 yrs BCE - 2010 yrs (CE) with mean sedimentation rates of  $0.06 \text{ mm yr}^{-1}$ .

233

234 **3.3- Geochemical and geophysical analyses.** Al, As, B, Ba, Ca, Cd, Cr, Cu, Fe, K, Mg,  
235 Mn, P, Pb, Si, Sr, Ti, Zn, and Zr concentration were analyzed in 91 samples by optical  
236 emission spectrometry using inductively coupled plasma-atomic emission spectroscopy  
237 (ICP-OES; Thermo ICP-OES iCAP 6300 DUO-Thermo Fisher Scientific, Waltham,  
238 MA, USA) at the IPE-CSIC laboratories. Samples were previously digested with  $\text{HNO}_3$   
239 (9 ml) and  $\text{HCl}$  (3 ml) in a microwave oven 'BERGHOF MWS'. Total Hg concentration  
240 measurements were carried out by Atomic Absorption Spectrophotometry using an  
241 Advance Mercury Analyzer (AMA 254, LECO Company). This equipment is  
242 specifically designed for the direct mercury determination in solid and liquid samples  
243 without a need of sample chemical pre-treatment. Certified reference material (CRM)  
244 were used to determine the accuracy and precision of the Hg measurements (NCS  
245 DC87103, soil,  $[\text{Hg}] = 0.017 \pm 0.003 \text{ mg kg}^{-1}$ ). The repeatability was  $\text{Sr} \leq 15 \%$  and the  
246 relative uncertainty associated with the method ( $k = 2$ ) was  $\pm 20\%$ . All analyses were

247 run at least in triplicate. Total Carbon (TC), Total Organic Carbon (TOC) and Total  
248 Inorganic Carbon (TIC) had been previously determined with a LECO SC 144 DR  
249 elemental analyzer (Oliva-Urcia et al., 2018). TIC values were obtained by subtracting  
250 TOC from TC (Fig. 2).

251 Principal Component Analyses (PCA) were applied to reduce the large  
252 geochemical dataset into a smaller number of variables (i.e. principal components (PC))  
253 helping to interpret environmental and depositional processes. PCA was carried out  
254 including all the elements (Cu, Zn, Cd, Mn, Ca, Fe, P, As, Hg, Pb, Sr, Zr, Si, Cr, Mg, Ti,  
255 B, K, Al and Ba) using trace metals' concentrations (Fig. 3) and accumulation rates  
256 (Fig. S1). The PCA was performed with varimax rotation over the geochemical dataset  
257 using the SPSS 23.0 software. To calculate Enrichment Factors (EFs), firstly, all the  
258 PTHE have been normalized to aluminum (Al) in order to confirm that the changes in  
259 metals concentrations are not related to detrital input variability. Al has been selected for  
260 normalization since this lithogenic element is immobile (i.e. geochemically stable) in  
261 the sediments and it is abundant in carbonated watersheds (Boës et al., 2011; Tylmann,  
262 2005). Later, EFs have been calculated using the average element concentrations before  
263 1000 BCE as baseline conditions which may differ from natural background values. EFs  
264 have been estimated to identify and quantify anthropogenic interferences in natural  
265 element cycles (Amos et al., 2015; Biester et al., 2007; Weiss et al., 1999).

266

$$267 \quad EF = \frac{[M_{cm}]/[Al_{cm}]}{[M_{bottom}]/[Al_{bottom}]}$$

268

269  $[M_{cm}]$  and  $[Al_{cm}]$  represent the metal and aluminum fluxes at the same depths of the  
270 sediment cores while  $[M_{bottom}]$  and  $[Al_{bottom}]$  are the metal and aluminum fluxes in the

271 basal sediments of the sediment cores in LM. Hg EF has been calculated as the ratio  
272 between the [Hg] in a given sample by the average [Hg] in the section below 1000 BCE  
273 following Biester et al. (2007)

274

275 **3.4- Pb isotopic analyses.** Pb isotope ratios are commonly used as tracers of both  
276 natural and anthropogenic sources of metals recorded in natural archives (Komárek et  
277 al., 2008). In order to shed light on the origin of Pb pollution found in the LM record,  
278 45 samples were collected for Pb isotopic analyses. A 0.1 g of powdered rock was  
279 digested overnight in HNO<sub>3</sub> and evaporated to dryness. The residue is dissolved in 0.5  
280 M ammonium acetate, and Pb separated of the major cations by conventional ion-  
281 exchange chromatography (DigiSEP Blue, SCP Science). The recovered Pb is  
282 evaporated to dryness, dissolved in 0.5 M HNO<sub>3</sub> and diluted to a final concentration of  
283 100–200 ppb. The samples were measured using the standard bracketing method. ICP-  
284 MS measurements were carried out with an Element 2 SF-ICP-MS (Thermo Finnigan,  
285 Bremen, Germany) equipped with a guard electrode to eliminate secondary discharge in  
286 the plasma and to enhance overall sensitivity. The high resolution double focusing  
287 (reverse Niers–Johnson geometry) single collector ICP-MS instrument provides flat top  
288 peaks in the low resolution mode ( $m/\Delta m$  300) which was used for the analysis of <sup>202</sup>Hg,  
289 <sup>204</sup>Pb, <sup>206</sup>Pb, <sup>207</sup>Pb and <sup>208</sup>Pb. A micro volume autosampler (SC-2 DX FAST  
290 Autosampler, ESI Inc., Omaha, NE, USA) and a sample introduction kit consisting of a  
291 PFA microflow nebulizer, a Peltier-cooled spray cyclonic chamber and a sapphire  
292 injector tube (ESI Inc., Omaha, NE, USA) were employed to transport the samples into  
293 the plasma of the ICP-MS. This configuration increases the sensitivity and stability of  
294 the conventional sample introduction setup. Samples were diluted ten times with 2 %  
295 (v/v) high purity HNO<sub>3</sub> to reduce the risk of clogging. The solutions were introduced

296 into the plasma using a PFA nebuliser, operating in self-aspiration mode at a flow rate of  
297 50 mL/min. Regarding reagents and standards, all the solutions were prepared with high  
298 purity water (18.2 MV cm) from Milli-Q element system designed for ultra-trace  
299 analysis (Millipore, Milford, MA, USA). Nitric acid (65%, analytical-reagent grade,  
300 Scharlab, Barcelona, Spain) was further purified by sub-boiling distillation (DST-1000  
301 Sub-Boiling Distillation System, Savillex Corporation, USA). Standard calibration  
302 solutions were prepared by appropriate dilution of a dissolved amount of NIST 981  
303 certified standard (Inorganic Ventures) with 2% high-purity nitric acid.

304

## 305 **4- RESULTS AND DISCUSSION**

306

### 307 **4.1. Concentrations and depositional processes of trace metals in LM.**

308

#### 309 4.1.1. Recent depositional processes: ice phenology, run-off and lake processes

310

311 Recent sediments in the deeper areas of LM characterized with sediment traps consist of  
312 siliciclastic silt, with about 1.1 % TOC, no carbonate and 0.05 % TS. Although  
313 carbonate-bearing formations occur in the watershed and the moraine deposits, the  
314 sediments in the lake are mostly devoid of carbonates (Oliva-Urcia et al., 2018).  
315 Mineral composition of the sediments is dominated by quartz, micas and detrital clay  
316 minerals, with presence of minor sulfides and other heavy minerals (mainly titanium  
317 oxides and zircon), all more resistant to weathering processes. Based on sediment traps  
318 data, the calculated sediment fluxes range between  $390 \text{ g m}^{-2} \text{ yr}^{-1}$  in the more proximal  
319 zones closer to the NW inlet to  $250 \text{ g m}^{-2} \text{ yr}^{-1}$  in the more distal areas. Microscope smear  
320 slide observations of recent sediments show the sporadic presence of heavy minerals in

321 the sediments (pyrite, galena, sphalerite and barite) indicative of occasional  
322 contributions from the watershed. High- Fe and Zn values have been found in the water  
323 column analysis in the thermocline in the ice-free period, being interpreted as a result of  
324 weathering reactions involving sulfides in the watershed (Sánchez-España et al., 2018).  
325 However, the influx of heavy metals into the lake due to run-off processes is expected to  
326 be small and likely constant during the last millennia as the composition of the surface  
327 sediment in LM drainage are remained the same in spite of glacier advances and retreats  
328 outside the watershed retreat (García-Ruiz et al., 2015).

329         The Iberian Peninsula has experienced different climatic periods during the Late  
330 Holocene (namely the Ibero-Roman Humid Period (IRHP), Dark Ages Cold Period  
331 (DACP, also known as Late Antiquity LIA, LALIA), Medieval Climate Anomaly  
332 (MCA), Little Ice Age (LIA) and Recent Warming) that most likely affected the annual  
333 duration of ice cover (i.e. ice phenology) in Spanish alpine lakes as it has been shown  
334 for the most recent phases (Sánchez-López et al., 2015). Ice phenology variability might  
335 have influenced differently the trace metal concentrations in LM sediments since the  
336 lake remains frozen about eight months per year (Sánchez-España et al., 2018). Direct  
337 atmospheric deposition of trace metal to the lake surface is hindered during cold periods  
338 when the lake is frozen and deposited metals would accumulate in the ice layer until  
339 discharged into the lake following ice melting. A similar process has been interpreted  
340 for pollen rain content during the late glacial and beginning of the Holocene (Leunda et  
341 al., 2017) as well as in other lakes in polar regions (Rodríguez-Pérez et al., 2019). In the  
342 case of mercury deposited on the ice and snow, it could also undergo re-emission to the  
343 atmosphere following heterogeneous photochemistry on the ice surface and/or  
344 snowpack (Angot et al., 2016). This process would release a fraction of the ice-trapped  
345 Hg back into the atmosphere contributing to lower atmospheric deposition of Hg to the

346 lake. On the contrary, large re-emission of other trace metals such as Pb, Cu, As and Zn  
347 from ice lake surface is not expected since these elements are largely immobile and  
348 would be remobilized during ice-melting and stored in the natural sink (i.e. the lake).  
349 Additionally, trace metals deposition in the Southern Pyrenees mainly occurs during the  
350 warm season when inland air masses enriched in trace elements and a thicker  
351 atmospheric mixed layer occurs (Bacardit and Camarero, 2009). Ice phenology would  
352 also affect the lake's annual stratification patterns and thus trace metals mobility in the  
353 water column. This process would affect Zn and, to a lesser extent, Cu and As (Sánchez-  
354 España et al., 2018). Nevertheless, we do not expect that this seasonal process would  
355 affect the annual depositional flux of these elements.

356

#### 357 4.1.2 Principal Component Analyses of the geochemical dataset.

358

359 PCA applied over the geochemical dataset (trace metal concentration and accumulation  
360 rates). PCA on trace metal concentration shows four main eigenvectors representing  
361 81.84 % of the matrix variance (Table 2). These eigenvectors explain the main  
362 environmental factors controlling sediment deposition and lake's endogenic and  
363 allochthonous processes. Factor loadings of each element in the extracted eigenvectors  
364 (PCs) and PCs variability are shown in Figs. 3 and 4 and Fig. S1 highlighting the  
365 fractionation of the communalities. Both PCA using trace metal concentration and  
366 accumulation rates show similar variances and grouping of geochemical elements (Figs.  
367 3 and S1; Tables 2 and S1).

368 The first component (PC1 46.7% of the variance) is related to lithogenic  
369 elements (Zr, Sr, Si, Cr, Mg, Ti, B, K, Al and Ba) and represents the delivery of  
370 allochthonous material to the lake via watershed run-off. Periods of increased run-off



371 occurred between 910-650 BCE, 160 BCE-30 CE, 660-830 CE and 1650-1770 CE most  
372 likely related to periods with higher snow cover in winter and/or increase snowmelt in  
373 summer. The second component PC2 (19,57 % of the total variance) is characterized by  
374 large positive loadings of Hg (0,90) and Pb (0,77), and moderate positively loadings of  
375 Cu (0,73), As (0,71), Cd (0,64) and Zn (0,59). PC2 suggest atmospheric deposition as  
376 the main process controlling the sediment enrichment of PHTE. PC2 show relatively  
377 low values during the IA while reached high values during the RP particularly between  
378 60-200 yrs CE. PC2 strongly decreased during the EMA and progressively increased  
379 since the onset of the HMA reaching maximum values at the end of the 19<sup>th</sup> century  
380 (Fig. 4). PC2 progressively increased during the Little Ice Age when colder conditions  
381 occurred in the Pyrenees (Morellón et al., 2012) suggesting climate influence on Hg  
382 deposition since PC2 is dominated by Hg. Thus, increased Hg levels during the LIA  
383 could result from lower re-emission of the Hg deposited on the snow/ice covering the  
384 lake surface and the catchment and enhanced transfer to the sediment during thawing  
385 events. Major increases in PC 1 and 2 show large temporal dissimilarities suggesting  
386 that the main trace metal pollutants input by weathering and run-off are not the main  
387 environmental processes driving hazardous trace metal pollutants in the lake.

388         The third component (PC3, 8.69% of the variance) is mainly characterized by  
389 positive loadings of TOC, Fe and P and reflects the accumulation of organic matter in  
390 the lake's bottom and nutrients input. Recent limnological surveys in the lake  
391 documented some variability in the biological activity in LM waters, although TOC  
392 values in the water column are extremely low (ranging from 0.3 mg/L to 1.2 mg/L  
393 (Sánchez-España et al., 2018)). Therefore, PC3 fluctuating values during the last 3000  
394 years would therefore reflect the variability in lacustrine primary production. PC4 (6.88  
395 % of the variance) is related to large positive loading of Ca, Mn and Cd. No carbonate

396 precipitates in the lake as the water column is undersaturated in calcite (Oliva-Urcia et  
397 al., 2018; Sánchez-España et al., 2018). Therefore, PC4 may reflect carbonate fluxes in  
398 the lake conditioned by the variable dissolution rate of carbonate particles from the  
399 watershed, controlled by water temperatures during the summer (Oliva-Urcia et al.,  
400 2018). Redox variability in the hypolimnion could also affect Mn and Cd as they are  
401 sensitive to redox-driven cycling in lacustrine systems (Hamilton-Taylor and Davison,  
402 1995). PC4 shows relatively stable values suggesting that the lake has been well  
403 oxygenated during the last 3 millennia, similarly to recent years when limnological  
404 surveys have documented a well oxygenation of the lake's water column throughout the  
405 annual cycle (Sánchez-España et al., 2018). PC4 peaks at 950 yrs BCE, 100 yrs BCE  
406 and 2000 yrs CE are more likely to respond to detrital carbonate accumulation in the  
407 lake since Mn is mostly linked to Ca-rich laminae in the Marboré sediments (Oliva-  
408 Urcia et al., 2018).

409         The moderate loadings of As and Zn in PCs 3 and 4 suggest that these elements  
410 can be either i) mobilized and re-precipitated in the sediment under anoxic/oxic changes  
411 in the hypolimnion and/or ii) fixed in organic compounds. Nevertheless, the continuous  
412 oxygenation of the hypolimnion and the very reduced biological activity (TOC in the  
413 sediment <1%) in this lake suggest that both factors do not have a significant influence  
414 on these elements variability during the Late Holocene. The lack of correlation between  
415 Hg and Pb with lithogenic and redox-sensitive elements and TOC also suggests that  
416 watershed runoff, redox variability and biological activity are not the main contributors  
417 to these major pollutant contents and fixation in the sediment. Therefore, although it  
418 may be a baseline deposition of some trace metals due to the weathering in the basin  
419 and run-off processes, the increase in PHTE would be mainly related to higher  
420 atmospheric deposition due to human activities at a local to subcontinental scale.

421

422 4.1.3 Temporal trace metal's concentration evolution

423

424 Hazardous trace metals follow different down-core concentration evolutions in the  
425 upper 175 cm of the analyzed sediment cores (Fig. 2). Pb concentration increased  
426 progressively during the IA with mean [Pb] of 14.8 mg kg<sup>-1</sup>. [Pb] abruptly increased at  
427 the onset of the RP reaching maximum values between 50- 210 yrs CE. During this  
428 period mean [Pb] of 46 mg kg<sup>-1</sup> are above the Pb TEC (Threshold Effect Concentration)  
429 guidelines in freshwater sediments (MacDonald et al., 2000), i.e. above the threshold  
430 from which harmful effects on ecosystems are likely to be observed. Low [Pb] values  
431 were recorded during the EMA and the HMA, with values of 19.6 mg kg<sup>-1</sup> and 18.6 mg  
432 kg<sup>-1</sup> respectively, although [Pb] did not return to pre-roman values. Higher [Pb]  
433 occurred during the LMA ([Pb] of 21.7 mg kg<sup>-1</sup>) and the MP ([Pb] of 25.6 mg kg<sup>-1</sup>)  
434 reaching the highest values during the IP, when [Pb] of 46 mg kg<sup>-1</sup> resemble the Pb  
435 values recorded during the RP. Arsenic showed increasing concentration values from the  
436 onset of IA to the end of the RP reaching a maximum concentration peak of 11 mg kg<sup>-1</sup>.  
437 Then it progressively decreased until the end of the HMA and showed elevated and  
438 fluctuating values during the MP and the IP with mean [As] of 10.8 mg kg<sup>-1</sup> (above [As]  
439 TEC values). Zn and Cu concentration progressively increased during the last 3000  
440 years with mean values of 74.2 and 4.7 mg kg<sup>-1</sup>, respectively. Mercury concentrations  
441 remained low until the end of the Middle Ages (0.018 mg kg<sup>-1</sup>), increased during the MP  
442 (0,027 mg kg<sup>-1</sup>) and doubled during the IP (0.054 mg kg<sup>-1</sup>).

443

#### 444 **4.2- Atmospheric transport of major pollutants.**

445 Air masses back trajectories reaching LM were computed to investigate the atmospheric  
446 transport of main pollutants from the main mining districts in the Iberian Peninsula (Fig.  
447 1). The analyses of back trajectories reaching LM reveal that 50 % of air masses come  
448 from SW France and the Ebro valley (Table 1). Air masses sources progressively  
449 decrease southward with Central and Western Spain contributing to 16.4 % of total air  
450 masses in the region, Southern Spain (17.4 %) and Northern Africa (3 %). Air masses  
451 from the Atlantic Ocean or emitted in the Central Iberian Peninsula are usually  
452 displaced to the Western Mediterranean Sea due to the westerlies flows. Once in this  
453 region, air masses can be trapped and funneled through the Ebro valley impacting in the  
454 Pyrenean mountain range. Likewise, Northern African air masses reach the Western  
455 Mediterranean basin and subsequently transported to the Pyrenees funneled through the  
456 Ebro valley. Other pathways are possible, such as the direct arrival through the Iberian  
457 Peninsula or, indirectly, through the Atlantic Ocean eventually reaching the Pyrenees  
458 from the south. Air masses back trajectories indicate that the transport from emission  
459 sources in central and southern Iberian Peninsula (e.g. Almadén, Rio Tinto, Cartagena,  
460 Linares) is not direct and would follow the Western Mediterranean route.

461 On the other hand, changes in atmospheric patterns, particularly related to the  
462 intensity of winds could have played an effect on delivery of trace metals from southern  
463 Spain during past climate phases in the Late Holocene (Le Roux et al., 2012; Martínez  
464 Cortizas et al., 2020; Sánchez-López et al., 2016). Indeed, the Roman Period  
465 experienced an E-W humidity gradient marked by an interplay between negative North  
466 Atlantic Oscillation (NAO) and positive East Atlantic (EA) phases. These changes in  
467 the atmospheric teleconnection patterns might result in different air masses trajectories

468 making different sources areas of metal pollution possible. Therefore, changes in the  
469 provenance of air masses is likely making alternative sources areas of metal pollution  
470 plausible. Inter-annual and multiannual variations in North Africa dust emissions have  
471 been extensively related to variability in atmospheric modes, such as the NAO and the  
472 ENSO (El Niño–Southern Oscillation) (Pey et al., 2013; Rodríguez et al., 2015;  
473 Salvador et al., 2014) when NAO positive phase occurs, the probability of transporting  
474 air masses from North Africa towards the IP is higher. Nevertheless, air masses  
475 travelling long distances usually move in upper layers, i.e. emissions from surface in the  
476 atmospheric boundary layer reach the free troposphere and then are transported by the  
477 westerlies flows. High altitude LM would therefore record the impact of long-range  
478 transport of trace metals-bearing air masses travelling in the free troposphere from  
479 southwestern Europe.

480         Global atmospheric Hg lifetime against surface deposition is estimated to be in  
481 the range of 3 to 6 months (Horowitz et al., 2017). Therefore, it is very likely that major  
482 Hg extractive episodes in Almadén resulted in high deposition in LM area. Indeed, 9.5%  
483 of the total back-trajectories arriving to LM pass over Almadén region (Table 1).  
484 Regarding other more immobile elements such as Pb, Zn, As or Cu, several studies have  
485 quantified the modern atmospheric transport of PHTE related to mining operations to  
486 determine how far the pollutants could travel from the emission sources (Asif et al.,  
487 2018; Csavina et al., 2012). These investigations documented the exponential fall of As,  
488 Zn and Pb concentration values with the distance from the mining site. Residence times  
489 of mining related-atmospheric particles might be limited to hours when PHTE would  
490 travel hardly beyond a few dozens of km except for minimum quantities. Several ore  
491 deposits are located within this distance to LM, as the Spanish Ag, Pb and Cu mines  
492 from Bielsa and Benasque and the French Montaignu mines, where Ag and Pb have been

493 exploited in ancient times (Calvo, 2008; Girard et al., 2010; Pérez et al., 2008). Ore  
494 extraction in larger Ag-Pb and Cu Pyrenean mines such as Arditurri or Banca, in the  
495 Basque Country and Southwestern France respectively has also been documented since  
496 Roman times (Ancel et al., 2001; Thalacker, 1804). Nevertheless, back trajectories  
497 results demonstrate that the emissions from large-scale mining districts located in  
498 Southern Spain can easily reach LM in less than three days (Fig. 1) depositing PHTE in  
499 the lake. Indeed, Rio La Carolina-Linares, Mazarrón-Cartagena and Río Tinto mines  
500 source areas represent 8.5, 8.4 and 7 % respectively. Therefore, the few air masses from  
501 the southern mining districts could rapidly transport the metals emitted during metal  
502 extraction activities and being eventually recorded in LM sedimentary archive.

503

### 504 **4.3- Sources and environmental impact variability of mercury, silver, lead and** 505 **copper mining**

506

#### 507 4.3.1 Lead

508

509 Positive Pb EF was found during several periods of the last 3000 years (Fig. 4). Pb EF  
510 and Pb<sub>flux</sub> remained low until 700 BCE and progressively increased since then until a  
511 maximum in 460 yrs BCE (Pb EF 2, Pb MAR  $12.7 \times 10^3 \mu\text{g m}^2 \text{yr}^{-1}$ ) and progressively  
512 decrease afterwards. Pb EF peaked again at 140 BCE (Pb EF 1.8, Pb MAR  $20.6 \times 10^3$   
513  $\mu\text{g m}^2 \text{yr}^{-1}$ ). Maximum Pb EF was found during the RP between 20 and 375 yrs CE (Pb  
514 EF 3.5, Pb MAR  $31 \times 10^3 \mu\text{g m}^2 \text{yr}^{-1}$ ). Maximum peaks occurred at 50 yrs CE (Pb EF  
515 4.5, Pb MAR  $37.5 \times 10^3 \mu\text{g m}^2 \text{yr}^{-1}$ ) and 180 yrs CE (Pb EF 5, Pb MAR  $38.5 \times 10^3 \mu\text{g}$   
516  $\text{m}^2 \text{yr}^{-1}$ ). Pb EF progressively decreased since the end of the RP reaching minimum  
517 values similar to natural baseline conditions between 750-870 yrs CE. Pb EF increased

518 at the onset of HMA at 950 yrs CE and remained high (mean values of 1.6) until 1350  
519 yrs CE (Pb EF 1.8, Pb MAR  $15 \times 10^3 \mu\text{g m}^2 \text{yr}^{-1}$ ). Low Pb levels occurred between  
520 1500 and 1820 yrs CE (Pb EF 1.5, Pb MAR  $17.5 \times 10^3 \mu\text{g m}^2 \text{yr}^{-1}$ ) reaching minimum  
521 enrichment (1.1) at 1700 yrs CE that resembles natural background values. During the  
522 IP Pb EF was very high (Pb EF 4.1, Pb MAR  $39.3 \times 10^3 \mu\text{g m}^2 \text{yr}^{-1}$ ) with maximum  
523 values at 1880 yrs CE (Pb EF 6.3, Pb MAR  $51.2 \times 10^3 \mu\text{g m}^2 \text{yr}^{-1}$ ). As and Zn follows  
524 the same trend than Pb suggesting a common source since both elements are by-  
525 products of ore exploitations from local veins enriched in galena, fluorite and sphalerite  
526 minerals

527

#### 528 *4.3.1.1 Iron Age*

529

530 The Pb isotopic dataset show a large variability across a well-defined mixing line (Fig.  
531 5).  $^{208}\text{Pb}/^{206}\text{Pb}$  and  $^{207}\text{Pb}/^{206}\text{Pb}$  ratios show the lowest (geogenic) values during the IA  
532 thus suggesting that Pb concentrations during this interval may reflect natural sources.  
533 Small increases in Pb EF during the 6<sup>th</sup> and 3<sup>rd</sup> centuries BCE may reflect ore extraction  
534 from the region of Murcia in Spain (Cartagena/Mazarrón mines) in agreement with  
535 previous archaeological and paleolimnological findings from coastal lagoons in Western  
536 Mediterranean that recorded the environmental impact related to the intense mining  
537 activities in the Cartagena mining district (Elbaz-Poulichet et al., 2011; Manteca et al.,  
538 2017).

539

#### 540 *4.3.1.2 Roman Period*

541

542 The large increase in Pb during the Roman Empire also coincides with the highest  
543 (anthropogenic)  $^{208}\text{Pb}/^{206}\text{Pb}$  and  $^{207}\text{Pb}/^{206}\text{Pb}$  isotopic ratios. The agreement of the  
544 isotopic values between 50 and 375 CE and the isotopic Pb signature from local high-  
545 altitude ore deposits from nearby mines (i.e. Parzán, Bizielle, Cierco, Palouma) might  
546 suggest the exploitation of Pb and Ag in high alpine environments in the Central  
547 Pyrenees during the Roman Period.  $^{208}\text{Pb}/^{206}\text{Pb}$  and  $^{207}\text{Pb}/^{206}\text{Pb}$  isotopic ratios during the  
548 RP are similar to those during the turn of the last century when Parzán mines were  
549 largely exploited (Fanlo et al., 1998; Nieto-Callen, 1996), suggesting a plausible Roman  
550 exploitation of these mines. Nevertheless, in spite of the geochemical similarities of LM  
551 signatures for Roman and recent mining compared to regional sites, the LM isotope  
552 signatures do not allow a clear adscription to local PHTM mining sources since we  
553 cannot disentangle local and regional mining from other regional pollution sources.

554 In our opinion, the anomalously high Pb levels during the Roman Empire imply  
555 that most of the trace metal pollution came from large-scale regional mining rather than  
556 local sources. Several indicators suggest that the exploitation of ore resources in high  
557 alpine areas from the Southern Central Pyrenees would have remained very local (if  
558 any) resulting in very reduced metal smelting and associated pollution during this  
559 period:

560 i) The absence of historical records documenting Roman mining in this region.  
561 Indeed, Roman mining is often associated to the development of large  
562 infrastructures to favor transport of metal resources which are not known in the  
563 area. As an example, Arditurri silver mines exploitation during roman times  
564 come with the development of large associated infrastructures for trading  
565 (Irabien et al., 2012; Urteaga, 2014).



566 ii) Mining procedures used in these exploitations required a continuous supply of  
567 goods for metal roasting and smelting which frequently results in large regional  
568 environmental impacts (i.e. deforestation and fires) (Pèlachs et al., 2009). Such  
569 environmental impacts (i.e. pollen indicators of deforestation, major increases in  
570 charcoal as indicator of biomass burning) have not been documented in regional  
571 and local paleoenvironmental reconstructions (González-Sampériz et al., 2017;  
572 Leunda et al., 2017; 2020) (Fig. 6). Additionally, studies in charcoal kilns from  
573 high altitude areas of the Pyrenees documented that charcoal production for ore  
574 smelting was likely very localized in time and space (Pèlachs et al., 2009).

575

576 A unique feature of the LM Pb record compared to other Pyrenean records is that the  
577 maximum pre-industrial Pb occurred during the Roman period, synchronous to an  
578 alpine peatbog record from Northern Central Pyrenees (Hansson et al., 2017), but not  
579 with other sites in Eastern and Western Pyrenees, where maximum Pb levels appeared  
580 later at 660-680 yrs CE (Camarero et al., 1998; Irabien et al., 2012). The anomalously  
581 high Pb concentration in LM and the absence of large mining operations in the Central  
582 Pyrenees suggest that most of the trace metal pollution came from other large-scale  
583 regional mining sources. Southern Spain hosts the most important Ag and Pb mines  
584 from the Ancient World. It has been calculated that about 70% of the total atmospheric  
585 Pb released to the environment during Roman times worldwide could be assigned to the  
586 Rio Tinto and Mazarrón source areas (Rosman et al., 1997). Therefore, increased Pb  
587 fluxes during the RP might reflect the signal of large-scale mining in southern Spain.  
588 Indeed, the isotope values of LM samples for the last 3000 years fall along a mixing line  
589 between two main end-members defined by Mazarrón-Cartagena and Rio Tinto mining  
590 districts. Those LM samples from the IA show mostly a composition similar to

591 Mazarrón-Cartagena mining district, while isotopic values during the RP have a larger  
592 range that could be an indication of more varied sources during that time, including a  
593 higher influence of Rio Tinto as well as higher input of lead from the lake's watershed  
594 via run-off. Northwestern Spain would also constitute alternative metal pollution  
595 sources since mining activities have been well documented in the area (Martínez-  
596 Cortizas et al., 2013). Nevertheless, their contribution to the Lake Marboré Pb record  
597 are expected to be very reduced.

598         The environmental impact of Roman mining has also been detected in other  
599 natural archives in the French Pyrenees, and Northwestern and Southern Spain (e.g  
600 (García-Alix et al., 2013; Hanebuth et al., 2018; Hansson et al., 2017; Hillman et al.,  
601 2017; Kylander et al., 2005; Manteca et al., 2017; Martín-Puertas et al., 2010; Martínez-  
602 Cortizas et al., 1997; 2013; Pontevedra-Pombal et al., 2013)). Nevertheless, those  
603 records show variable timing and magnitude due to their location with respect to the  
604 emission sources. Thus, while LM Pb record agrees very well with Pb levels recorded in  
605 peatbogs from the Northern Central Pyrenees (Hansson et al., 2017) (Fig. 6) as well as  
606 with Pb levels recorded in coastal sediments from NW Mediterranean (Portlligat bay,  
607 270 km east from LM) (Serrano et al., 2011). In the other hand, Pb levels in Lake Zoñar  
608 (Southern Spain) showed maximum values between 500 and 100 yrs BCE due to  
609 extensive mining in Southern Iberian Peninsula by Iberians, already influenced by  
610 Greeks and Phoenicians (Fig. 6) (Martín-Puertas et al., 2010). Further timing  
611 discrepancies have been found with other high-altitude pollution and remote records in  
612 the Alps (Cold du Dome ice core Western Alps (Preunkert et al., 2019)) and Greenland  
613 (NGRIP2 (McConnell et al., 2018)) (Fig. 6). This asynchrony in maximum Pb levels  
614 underlines the variable influence of diverse emission sources in each location.  
615 Greenland ice core records would represent the whole European emissions and Western

616 Alps ice cores would record mostly emissions from France and Northern  
617 Mediterranean. On the other hand, LM would record PHTM emissions mostly from the  
618 main mining districts from Southwestern Europe representing the atmospheric Pb levels  
619 during the RP at a regional to sub-continental scale because of the privilege location of  
620 LM in the free troposphere. Indeed, the high Pb content in the atmosphere was a major  
621 health concern in the Iberian Peninsula during Roman times affecting Iberian population  
622 as recorded in the Pb isotopic composition of human bones from living individuals in  
623 NW Iberian Peninsula (López-Costas et al., 2020).

624 Pb concentrations and  $^{208}\text{Pb}/^{206}\text{Pb}$  and  $^{207}\text{Pb}/^{206}\text{Pb}$  isotopic ratios progressively  
625 declined since the end of the 2<sup>nd</sup> century CE coinciding with the decrease of Roman  
626 mining in the Iberian Peninsula, largely attributed to the socio-economic crises of the  
627 Roman Empire. These economic crises started with the Antonine plague that disrupted  
628 mining through high mortality and decreased demand as well as with the reduced silver  
629 content used in coinage in the 3<sup>rd</sup> century CE (McConnell et al., 2018). During EMA,  
630 the proximity of the mines to population settlements was a significant factor for mine  
631 abandonment due to the transportation costs and because local miners adopted methods  
632 and infrastructure less efficient than those of Roman times (Martinon-Torres and  
633 Rehren, 2011).

634

#### 635 *4.3.1.3 Last millennium*

636

637 An increase in Pb EF and MAR and a shift towards more radiogenic values occurred  
638 during the HMA and LMA most likely related to the renew mining activities and the  
639 exploitation of more local mines as Parzán (Fig. 1). This period coincides with  
640 widespread innovations in mining and refining processes in Europe to reach the high

641 demands of the increasing European population between 11-13<sup>th</sup> centuries. The Pb peak  
642 at the second half of the 12<sup>th</sup> century coincides with the first historical evidences of local  
643 mining in Parzán when Aragonese King Alfonso II conceded official privileges of  
644 exploitation of the Bielsa mines to the local people (Bielza de Ory, 1983). The decline  
645 of Pb levels since 1350 CE recorded in LM sediments coincides with the interrupted  
646 metal production in Europe during the Black Death Pandemic (1349-1353 yrs CE) that  
647 dropped atmospheric Pb to undetectable levels (More et al., 2017). Pb levels recovered  
648 afterwards, but remained low during the following centuries might be related to the  
649 onset of large-scale silver mining in South America. In this context, high alpine, small-  
650 scale silver mines such as the ones in the Axial Pyrenees were less profitable and  
651 probably intermittently abandoned. However, historical archives documented that more  
652 than 15000 kg of Pb were produced (and smelted in local kilns) in Parzán by the end of  
653 the 16<sup>th</sup> century (Nieto-Callen, 1996). Only at the end of the 19<sup>th</sup> century, Pb levels  
654 increased exponentially in LM (Fig. 6) and other Pyrenean lakes (Corella et al., 2017;  
655 2018) due to large-scale exploitation of Parzán mines (Fanlo et al., 1998; Nieto-Callen,  
656 1996).

657         The correspondence between atmospheric Pb levels and warmer climate phases  
658 during the last millennium suggests a connection between source availability (i.e. ore  
659 extraction and smelting) and depositional processes with climate. Thus, the Pb and Ag  
660 mining extractive period in the Pyrenees during the HMA and LMA coincided with the  
661 MCA, a warm and arid period in the Iberian Peninsula between 950 and 1350 yr CE  
662 (Moreno et al., 2012). Prolonged snow-free periods at the mining sites would have  
663 favoured ore resources exploitation in mountain areas. On the other hand, a return to  
664 almost baseline natural backgrounds of atmospheric Pb levels that occurred between the  
665 EMA and the MP coincided with the DACP and the LIA, known as cold periods in NE

666 Iberian Peninsula (Corella et al., 2012; 2013; Morellón et al., 2012) and Iberian  
667 mountains (Oliva et al. 2018). Atmospheric pollution levels were particularly low  
668 during the Maunder Minimum (1645-1715 yrs CE) when trace metals accumulation  
669 fluxes were greatly reduced (Fig. 4). Therefore, climate variability has been likely also a  
670 determinant factor controlling mining in high-alpine environments (e.g. Parzán mines  
671 located at > 2300 m a.s.l.) during the last centuries. The relation between past warmer  
672 climate phases and mining activities in high alpine environments was also observed in  
673 the western Alps (Guyard et al., 2007) where ore extraction became possible because of  
674 glaciers retreated in the region when temperature increased.

675

#### 676 4.3.2 Copper

677

678 Cu EF increased progressively reaching the highest values at the end of the IA at 360  
679 yrs BCE (Cu EF 2) (Fig. 4). Cu EF decreased during the first phase of the RP until 50  
680 yrs CE. Cu EF started to increase during the mid 4<sup>th</sup> century and peaked at the onset of  
681 the 5<sup>th</sup> century CE (410 yrs CE, Cu EF 3.2). Cu EF reduced during the EMA and  
682 increased during the HMA and LMA (Cu EF 2) with maximum Cu enrichment at 1200  
683 yrs CE (Cu EF 2.7). Cu EF remained high during the 16<sup>th</sup> century with mean Cu  
684 enrichment of 2.4. Cu EF decreased during the 18<sup>th</sup> century and increased again during  
685 the IP (Cu EF 2.6) peaking at the turn of the 19<sup>th</sup> century (Cu EF 3.4).

686         The first documented increase in copper concentrations in Greenland exceeding  
687 the natural levels occurred about 2500 years ago (Hong et al., 1996) and provides  
688 evidence for widespread copper mining during the Iron Age. The oldest presence of  
689 copper miners and metalworkers in the region was documented in the Montpellier  
690 region (Southern France) in the 3<sup>rd</sup> millennium BCE (Ambert et al., 2002) while large

691 copper mines were in operation in N Iberia since the Chalcolithic (De Blas, 2005; Vidal,  
692 2012; Martínez-Cortizas et al., 2016)

693         The Cu enrichment in LM during the 4<sup>th</sup> century BCE agrees well with an  
694 enrichment in Cu recorded in peatbogs sediments from Northern Central Pyrenees  
695 between 480–180 yrs BCE (Hansson et al., 2017) suggesting copper mining from the  
696 abundant Cu-rich ore deposits in the region (Calvo, 2008). The high Cu levels since 50  
697 yrs CE remained elevated during almost all Roman Empire most likely due to the highly  
698 polluting smelting technologies used for copper production during Roman times in  
699 Europe (Hong et al., 1996). This is in agreement with the roman exploitation of Banca  
700 mines (French Western Pyrenees), the largest roman copper mines in France, between  
701 1<sup>st</sup> century BCE and 4<sup>th</sup> century CE (Ancel et al., 2012; Urteaga, 2014). Nevertheless,  
702 the highest copper production in the Iberian Peninsula occurred in the Río Tinto region  
703 (SW Iberia) as well in other copper mines from NW Iberia (Wilson, 2002). Maximum  
704 atmospheric Cu levels between the mid 4<sup>th</sup> century and the early 5<sup>th</sup> century might  
705 reflect the increase in copper demand for coinage when Roman monetary system shifted  
706 to a bimetallic currency composed of a gold and copper alloy (McConnell et al., 2018;  
707 Wilson, 2002).

708         Copper levels increased again in LM record at around 1200 yrs CE and persisted  
709 high for almost five centuries. The enrichment in the early 13<sup>th</sup> century occurred almost  
710 one century before the first historical documents of copper mining in the area when  
711 kings Alfonso II and Jaime II conceded privileges for mineral extraction to local  
712 noblemen in the Pyrenean surrounding valleys as well as from Santa Eulalia la Mayor  
713 (60 km south of LM) in 1277 and 1293 yrs CE, respectively. The use of local kilns for  
714 Cu, Ag, Pb and Fe smelting practices were also documented during this time (Nieto-  
715 Callen, 1996). Cu levels decreased during the 18<sup>th</sup> century and peaked again in the 19<sup>th</sup>

716 century. This variability is in agreement with the historical local mining activities of the  
717 area that derived, on the one hand, in unsuccessful copper resources prospection during  
718 the 18<sup>th</sup> century and, on the other hand, the boost of copper mines in the region during  
719 the 19<sup>th</sup> century (Nieto-Callen, 1996).

720

#### 721 4.3.3 Mercury

722

723 Hg levels in LM showed a significant variability during the Late Holocene. Mercury EF  
724 and Hg<sub>flux</sub> were at the lowest levels until 620 yrs BCE (EF <1, 12.8  $\mu\text{g m}^2 \text{yr}^{-1}$ ) and  
725 remained high between 620–270 yrs BCE (Hg EF=1.2, Hg MAR=13.4  $\mu\text{g m}^2 \text{yr}^{-1}$ ). Low  
726 values were found until 20 yrs CE and then increased slightly increase during the RP.  
727 Hg EF remained stable until the MP, when Hg EF progressively increased with mean  
728 Hg EF values of 1.9 (Hg MAR=18,4  $\mu\text{g m}^2 \text{yr}^{-1}$ ) reaching maximum values during the  
729 IP (Hg EF=3.7, Hg MAR=40  $\mu\text{g m}^2 \text{yr}^{-1}$ ).

730 Hg emissions before the Industrial Period have been mostly attributed to  
731 historical mining, volcanic activity and coal burning (Cooke et al., (2020) and  
732 references therein). Periods of Hg levels in LM are not coherent with the impact of the  
733 main volcanic eruptions in the Northern Hemisphere, although the decadal  
734 chronological resolution of LM might have hindered the identification of volcanic  
735 episodes with large Hg emissions to the atmosphere (e.g. Vesubio volcanic eruption in  
736 79 CE coinciding with the higher Hg EF during the 1<sup>st</sup> century CE). Recent studies in  
737 the French Pyrenees and Southeastern France have suggested that atmospheric Hg  
738 deposition increase during the Medieval and the Modern Period was mostly caused by  
739 enhanced Hg emissions from biomass burning (Elbaz-Poulichet et al., 2011; Enrico et  
740 al., 2017). Nevertheless, Hg MAR and EF in LM does not coincide with major

741 deforestation and burning episodes in alpine environments from the Southern Central  
742 Pyrenees (González-Sampériz et al., 2017; 2019; Leunda et al., 2017; 2020) (Fig. 6).  
743 Therefore, Hg net fluxes recorded in LM would most likely be related to Hg emissions  
744 caused by local and/or regional mining activities.

745 Hg EF for the period 1000 BCE-1500 CE correlates well with Zn EF ( $\sigma=0,81$ )  
746 and, to a lesser extent, with Cu ( $\sigma=0,65$ ). This correlation suggests that Hg enrichments  
747 before the Modern Period might be related to the exploitation of i) local Pb (Ag)-Zn  
748 veins which are dominated by galena and sphalerite deposits (Subías et al., 2015) and/or  
749 ii) chalcopyrite exploited in local fire settings for copper extraction since these minerals  
750 can host significant Hg concentrations (George et al., 2018; Rytuba, 2003) which can  
751 eventually result in increased Hg emissions (as by-products) to the local atmosphere.  
752 Recent paleolimnological studies in the Alps have also highlighted the influence of local  
753 Cu and Pb-Ag ore exploitations controlling Hg enrichment in high alpine environments  
754 in ancient times (Elbaz-Poulichet et al., 2020). Nevertheless, we cannot exclude Hg  
755 emissions from regional sources (i.e. Almadén mines, Central Spain) since large-scale  
756 cinnabar mining in Almadén has been carried out during the last 2500 years (Hernandez,  
757 2007). Considering back trajectories analyses and atmospheric Hg residence times it is  
758 very likely that major Hg extractive episodes in Almadén resulted in an increase Hg  
759 accumulation in LM. Almadén's mining exploitation by Romans and Arabs resulted in  
760 large Hg release to the atmosphere. Indeed, the Roman writer Pliny the Elder wrote  
761 about the extraction of Hg (and its distillation in marmites) and its trade between Spain  
762 and Rome in the 1<sup>st</sup> century CE, while the Arabs intensified Hg production in Almadén  
763 with more than 1000 laborers working in the mines during the 11<sup>th</sup> century (Goldwater,  
764 1972).



765           The progressive increase in Hg EF and MAR that occurred in LM during the last  
766 500 years greatly differs from the other metal EFs evolution (Fig. 7) and follows the Hg  
767 historical production in Almadén documented during the last five centuries (Hylander  
768 and Meili, 2003). Hg production significantly increased in the 16<sup>th</sup> century due to the  
769 need for Hg amalgamation in silver mining in the Spanish colonies. As a result, large  
770 amounts of Hg dissipated to the environment. As an example, between 1571 and 1660  
771 yrs CE approximately 25000 tons of Hg were produced in the mines (Hylander and  
772 Meili, 2003). This likely resulted in a 30% increase in Hg MAR during this period (18.2  
773  $\mu\text{g m}^2 \text{ yr}^{-1}$ ) from the stable Hg MAR before the Modern Period (13.7  $\mu\text{g m}^2 \text{ yr}^{-1}$ ). A 25  
774 % decrease in Hg MAR at 1675 yrs CE could be explained by the drastic decrease in Hg  
775 Almadén production during the second half of the 17<sup>th</sup> century due to the exhaustion of  
776 Hg resources in Almadén (Bethell, 1984) and the reduction of Hg shipping to South  
777 America. Nevertheless, the discovery of new veins in Almadén at the turn of the century  
778 most likely explains the abrupt increase in Hg MAR during the early 18<sup>th</sup> century (22.6  
779  $\mu\text{g m}^2 \text{ yr}^{-1}$ ). Hg levels progressively increased during the Industrial period peaking at  
780 the turn of the 20<sup>th</sup> century (EF of ~4 and MAR of ~40  $\mu\text{g m}^2 \text{ yr}^{-1}$ ) and between 1960-  
781 1970 CE (EF of 4.8 and MAR 70  $\mu\text{g m}^2 \text{ yr}^{-1}$ ) when Hg production peaked at 10 000 tons  
782 per year (Hylander and Meili, 2003). The Hg variability pattern recorded in LM during  
783 the 20<sup>th</sup> century is similar to the recent Hg variability highlighted in multi-short cores  
784 studies in Southern Sweden and NW Spain (Bindler et al. 2004; Martínez-Cortizas et  
785 al., 2012).

786 The 2-fold decline in Hg MAR since 1970 CE coincides with a decreasing trend in Hg  
787 production in Almadén during the last decades (Fig. 7) until its closure in the 2000s.  
788 This 2-fold decrease in atmospheric Hg concentrations since the 1970s is in agreement  
789 with direct atmospheric monitoring and glacier firn records (EMEP; Faïn et al., 2009).

790 In the Iberian Peninsula, anthropogenic Hg release to the atmosphere due to  
791 mining activities in Almadén ca. 2500 years before present was first documented in peat  
792 cores from NW Spain (Martinez-Cortizas et al., 1999), estuarine sediments from  
793 Southwestern Spain (Leblanc et al., 2000) and marine sediments in the Western  
794 Mediterranean (Portlligat Bay) (Serrano et al., 2013). In the Pyrenees, atmospheric Hg  
795 fluxes have been previously reported in peat sediments from the French Pyrenees  
796 (Enrico et al., 2017) as well as in lake Montcortès in the Pre-Pyrenees located at 1031 m  
797 a.s.l. (Corella et al., 2017). LM Hg concentration and fluxes agree well with  
798 atmospheric Hg fluxes previously reported in peat sediments from the French Pyrenees  
799 (Enrico et al., 2017) as well as in low-elevation lake Montcortès sediments in the Pre-  
800 Pyrenees (Corella et al., 2017) highlighting the regional to sub-continental scale  
801 pollution recorded in these natural archives.

802

## 803 **5- SUMMARY AND CONCLUSIONS**

804

805 The geochemical Lake Marboré record allowed us to understand the atmospheric  
806 variability of hazardous trace metals related to historical mining and metalworking  
807 activities in the Iberian Peninsula during the Late Holocene. The location of the lake at  
808 2600 m a.s.l. makes it particularly sensitive to tropospheric transport of trace metals.  
809 Historical metallurgy has derived in a significant increase in Hg, Pb and, to a lesser  
810 extent, Zn, Cu and As during the Pre-Industrial Period constituting one of the oldest,  
811 large-scale anthropogenic impact on the environment. This historical atmospheric  
812 pollution has left a profound geochemical signature in the lake where several trace  
813 metals reach concentration levels that might have had ecotoxicological implications in  
814 these high-mountain ecosystems.

815           The multidisciplinary approach involving statistical, isotopic and meteorological  
816 re-analyses have also enabled the reconstruction of the history and sources of hazardous  
817 trace metal pollutions over the last 3000 years. Back trajectories analyses show that air  
818 masses capable of transporting atmospheric pollutants to Lake Marboré may come from  
819 almost all southwestern Europe and northern Africa in less than 3 days highlighting the  
820 sensitiveness of the lake to track environmental pollution sources at a local to sub-  
821 continental scale. Pb isotopic analyses suggest that Ag and Pb mining in South-eastern  
822 Spain might have been responsible for subtle trace metal enrichment during the Late  
823 Iron Age. Very high atmospheric Pb fluxes were found during the Roman Empire most  
824 likely related to the global rise of atmospheric Pb emission from Río Tinto and  
825 Mazarrón mines emplaced in Southern Iberia Peninsula. Isotope analyses suggest a  
826 contribution of small-scale ore exploitation from local, high-altitude mines but more  
827 archaeological surveys are needed as the assessment of all local sources is a critical  
828 issue when reconstructing the history of pollution using natural archives. Independently  
829 of the source we find evidence that atmospheric Pb levels were of the same magnitude  
830 that the ones found during the Industrial Period. Local Ag, Pb and Cu mining  
831 reactivated in the Central Pyrenees during the High Middle Ages when socio-economic  
832 conditions and mild-climates allowed ore extraction in high-alpine environments and all  
833 over the Iberian Peninsula. These local mining activities significantly decreased during  
834 the harsh climate conditions documented at the onset of the Little Ice Age. Contrarily,  
835 atmospheric Hg progressively increased during the Modern Period due to the large-scale  
836 production in Almadén mines in Central Spain, leading to high loads of Hg burden in  
837 Pyrenean sedimentary environments.

838           Lake Marboré record of past emissions related to mining and metalworking  
839 activities shows a common pattern with other European pollution records showing a

840 climax during the Roman period, Medieval times and since the Industrial Revolution.  
841 This agreement could be partly explained by the location of the lake above the mixing  
842 atmospheric boundary layer, therefore, recording long-range (inter-hemispheric)  
843 atmospheric pollutants transport. The lake's location in a high elevation area, as well as  
844 the watershed and limnological characteristics of Lake Marboré makes this site a unique  
845 record of past atmospheric contamination that highlights the usefulness of long-term  
846 pollution archives to contextualize current atmospheric pollution levels. Indeed, the  
847 environmental consequences and atmospheric Pb pollution in Antiquity are substantial  
848 and could even exceed present-day levels.

849         This study provides a further understanding of the pollution burden legacy in  
850 lacustrine sediments constitutes a significant environmental hazard for high-mountain  
851 ecosystems that should be adequately quantified and monitored. Our findings also  
852 contribute to the contextualization of current air metal pollution by reconstructing long-  
853 term (centennial to millennial-scales) atmospheric trace metal levels beyond the very  
854 few instrumental measurements that barely spans the last decades. Nevertheless, the  
855 determination of pollution sources presented in this study are not entirely conclusive.  
856 Follow-up studies on Lake Marboré focussed on Hg, Pb, Nd and Sr isotopes will shed  
857 more light on the provenance and biogeochemical cycling of the main pollutants  
858 deposited in the lake.

859

## 860 **6- ACKNOWLEDGMENTS**

861 Financial support has been received by the Sobrarbe Geopark through the project  
862 “Reconstrucción de la minería histórica en la Comarca del Sobrarbe y su impacto  
863 ambiental durante el Antropoceno”) and by the Spanish Ministry of Economy and

864 Competitiveness (MINECO) project MEDLANT (CGL2016-76215-R). This work is  
865 also supported by the FEDER funds through the INTERREG V-A Spain-France-  
866 Andorra (POCTEFA 2014-2020, REPLIM project, Ref. EFA056/15).

867

## 868 **7- FIGURE CAPTIONS**

869

870 **Fig. 1:** Frequency map of air mass back trajectories arriving to Lake Marboré (LM, blue  
871 circle). Yellow triangles indicate the location of historical mining sites mentioned in the  
872 text (1- Parzán; 2- Banca; 3- Arditurri; 4- Emporion; 5- Almadén; 6- Rio Tinto; 7- La  
873 Carolina-Linares; 8- Mazarrón-Cartagena).

874 **Fig. 2:** LM down-core evolution of Potential Harmful Trace Metal (PHTM) and  
875 aluminum concentrations, Organic Matter Content (TOC) and sediment density values.

876 **Fig. 3.** Communalities of the geochemical elements obtained from Principal Component  
877 Analyses (PCA).

878 **Fig. 4.** Principal Components eigenvectors (PC) and Enrichment factors (EF) and  
879 normalization (coloured area) of PHTM recorded in LM during the last 3000 years.  
880 Main historical periods are also indicated; Iron Age (IA), Roman Period (RP); Early,  
881 High and Late Middle Ages (EMA, HMA and LMA respectively); Modern Period and  
882 beginning of Contemporary Age (MP); Industrial Period (IP).

883 **Fig. 5.** Changes in  $^{208}\text{Pb}/^{206}\text{Pb}$  and  $^{207}\text{Pb}/^{206}\text{Pb}$  isotopic ratio in LM compared with other  
884 natural and anthropogenic (mining) sources. Different Pb isotopic values have been  
885 obtained from: Oxford archeological lead isotope database (OXALID) (Stos-Gale and  
886 Gale, 2009) for the Linares, Rio Tinto and Cartagena mines, Arditurri mines (Velasco et  
887 al., 1996), local galena mines from Emporion (NE Spain) (Montero-Ruiz et al., 2007),

888 ore deposits and local mines from Southern Central Pyrenees (Camarero et al., 1998;  
889 Girard et al., 2010; Subías et al., 2015).

890 **Fig. 6.** From bottom to top: Lead enrichment factor (EF), Pb Mass Accumulation Rates  
891 (MAR) during the last 3000 years; Calcite sublayering in Lake Montcortès as a proxy of  
892 prolonged winter conditions in Southern Central Pyrenees (Corella et al., 2012);  
893 Charcoal fluxes in LM and Lake Basa de la Mora sediment records as proxies of fires  
894 and human activities in the area (Leunda et al., 2020); Pb isotopic ratios in LM; Etant  
895 Mort Pb EF (redrawn from Hansson et al., (2017)); Lead content in western Alps (Col  
896 du Dome ice core (Preunkert et al., 2019)) and Greenland ice cores (McConnell et al.,  
897 2019). Coloured vertical bars represent the main climatic phases during the Late  
898 Holocene.

899 **Fig. 7.** Atmospheric mercury (Hg) deposition in the Central Pyrenees over the last  
900 millennium from LM (this study) and Montcortès (Corella et al., 2017) as well as  
901 estimations of mercury production in Spanish mines (Hylander and Meili (2003)). Main  
902 historical and climatic phases are also indicated.

903

## 904 **8- REFERENCES**

905 *Ambert. P., Coularou. J., Cert. C., Guendon. J.-L., Bourgarit. D., Mille. B.t.,*  
906 *Dainat. D., Houlès. N., Baumes. B., 2002. Le plus vieil établissement de métallurgistes*  
907 *de France (IIIe millénaire av. J.-C.): Péret (Hérault). Comptes Rendus Palevol 1. 67-74.*

908 *Amos. H.M., Sonke. J.E., Obrist. D., Robins. N., Hagan. N., Horowitz. H.M.,*  
909 *Mason. R.P., Witt. M., Hedgecock. I.M., Corbitt. E.S., 2015. Observational and*  
910 *modeling constraints on global anthropogenic enrichment of mercury. Environmental*  
911 *Science & Technology 49. 4036-4047.*

912 Ancel. B., Dardignac. C., Parent. G., Beyrie. A., 2001. *La mine de cuivre antique*  
913 *des Trois Rois à Banca, vallée de Baïgorry (Pyrénées-Atlantiques)*. Sablayrolles éd.  
914 179-194.

915 Ancel. B., Parent. G., Beyrie. A., Kammenthaler. E., Dardignac. C., 2012.  
916 *Stratégie d'exploitation et galerie d'exhaure dans la mine de cuivre antique de Banca*  
917 *(Pyrénées Atlantiques). L'eau: usages, risques et représentation dans le Sud-Ouest de la*  
918 *Gaule et le Nord de la péninsule Ibérique, de la fin de l'Âge du Fer à l'Antiquité tardive*  
919 21. 169-189.

920 Angot. H., Dastoor. A., De Simone. F., Gårdfeldt. K., Gencarelli. C.N.,  
921 Hedgecock. I.M., Langer. S., Magand. O., Mastromonaco. M.N., Nordstrøm. C., 2016.  
922 *Chemical cycling and deposition of atmospheric mercury in polar regions: review of*  
923 *recent measurements and comparison with models. Atmospheric Chemistry & Physics.*  
924 16. 10735–10763.

925 Appleby. P.G., 2001. *Chronostratigraphic techniques in recent sediments*. In:  
926 *Last. W.M., Smol. J.P. (Eds.). Tracking Environmental Change Using Lake Sediments.*  
927 *Volume 1: Basin Analysis, Coring, and Chronological Techniques. Kluwer Academic*  
928 *Publishers, Dordrecht, pp. 171-203.*

929 Asif. Z., Chen. Z., Han. Y., 2018. *Air quality modeling for effective environmental*  
930 *management in the mining region. Journal of the Air & Waste Management Association*  
931 68. 1001-1014.

932 Bacardit. M., Camarero. L., 2009. *Fluxes of Al, Fe, Ti, Mn, Pb, Cd, Zn, Ni, Cu,*  
933 *and As in monthly bulk deposition over the Pyrenees (SW Europe): the influence of*  
934 *meteorology on the atmospheric component of trace element cycles and its implications*  
935 *for high mountain lakes. Journal of Geophysical Research: Biogeosciences 114.*

936 *Bacardit. M., Camarero. L., 2010. Modelling Pb, Zn and As transfer from*  
937 *terrestrial to aquatic ecosystems during the ice-free season in three Pyrenean*  
938 *catchments. Science of the Total Environment 408. 5854-5861.*

939 *Bacardit. M., Krachler. M., Camarero. L., 2012. Whole-catchment inventories of*  
940 *trace metals in soils and sediments in mountain lake catchments in the Central*  
941 *Pyrenees: apportioning the anthropogenic and natural contributions. Geochimica et*  
942 *Cosmochimica Acta 82. 52-67.*

943 *Bethell. L., 1984. Colonial Latin America. Cambridge University Press.*

944 *Bielza de Ory. V., 1983. Estudio histórico geográfico del Valle de Bielsa."*  
945 *Colección.*

946 *Biester. H., Bindler. R., Martinez-Cortizas. A., Engstrom. D.R., 2007. Modeling*  
947 *the past atmospheric deposition of mercury using natural archives. Environmental*  
948 *Science & Technology 41. 4851-4860.*

949 *Bindler. R., Klarqvist. M., Klaminder. J., Förster. J., 2004. Does within-bog*  
950 *spatial variability of mercury and lead constrain reconstructions of absolute deposition*  
951 *rates from single peat records? The example of Store Mosse, Sweden. Global*  
952 *Biogeochemical Cycles. 18(3).*

953 *Boës. X., Rydberg. J., Martinez-Cortizas. A., Bindler. R., Renberg. I., 2011.*  
954 *Evaluation of conservative lithogenic elements (Ti, Zr, Al, and Rb) to study*  
955 *anthropogenic element enrichments in lake sediments. Journal of Paleolimnology 46.*  
956 *75-87.*

957 *Calvo. M., 2008. Minerales de Aragón. Prames. Zaragoza.*

958 *Camarero. L., 2003. Spreading of trace metals and metalloids pollution in lake*  
959 *sediments over the Pyrenees. Journal de Physique IV (Proceedings). EDP sciences. pp.*  
960 *249-253.*



961 Camarero. L.. 2017. *Atmospheric chemical loadings in the high mountain:*  
962 *current forcing and legacy pollution. High Mountain Conservation in a Changing*  
963 *World. Springer. Cham. pp. 325-341.*

964 Camarero. L.. Masqué. P.. Devos. W.. Ani-Ragolta. I.. Catalan. J.. Moor. H.C..  
965 Pla. S.. Sanchez-Cabeza. J.A.. 1998. *Historical Variations in Lead Fluxes in the*  
966 *Pyrenees (Northeast Spain) from a Dated Lake Sediment Core. Water. Air. and Soil*  
967 *Pollution 105. 439-449.*

968 Cooke. C.A.. Balcom. P.H.. Kerfoot. C.. Abbott. M.B.. Wolfe. A.P.. 2011. *Pre-*  
969 *Colombian mercury pollution associated with the smelting of argentiferous ores in the*  
970 *Bolivian Andes. Ambio 40. 18-25.*

971 Cooke. C.A.. Martínez-Cortizas. A.. Bindler. R.. Gustin. M.S.. 2020.  
972 *Environmental archives of atmospheric Hg deposition—A review. Science of the Total*  
973 *Environment 709. 134800.*

974 Corella. J.. Saiz-Lopez. A.. Sierra. M.. Mata. M.. Millán. R.. Morellón. M..  
975 Cuevas. C.. Moreno. A.. Valero-Garcés. B.. 2018. *Trace metal enrichment during the*  
976 *Industrial Period recorded across an altitudinal transect in the Southern Central*  
977 *Pyrenees. Science of the Total Environment 645. 761-772.*

978 Corella. J.P.. Brauer. A.. Mangili. C.. Rull. V.. Vegas-Vilarrúbia. T.. Morellón.  
979 M.. Valero-Garcés. B.L.. 2012. *The 1.5-ka varved record of Lake Montcortès (southern*  
980 *Pyrenees. NE Spain). Quaternary Research 78. 323-332.*

981 Corella. J.P.. Stefanova. V.. El Anjoumi. A.. Rico. E.. Giralt. S.. Moreno. A..  
982 Plata-Montero. A.. Valero-Garcés. B.L.. 2013. *A 2500-year multi-proxy reconstruction*  
983 *of climate change and human activities in northern Spain: The Lake Arreo record.*  
984 *Palaeogeography. Palaeoclimatology. Palaeoecology 386. 555-568.*

985 Corella. J.P., Valero-Garcés. B.L., Wang. F., Martínez-Cortizas. A., Cuevas. C.,  
986 Saiz-Lopez. A., 2017. 700 years reconstruction of mercury and lead atmospheric  
987 deposition in the Pyrenees (NE Spain). *Atmospheric environment* 155. 97-107.

988 Csavina. J., Field. J., Taylor. M.P., Gao. S., Landázuri. A., Betterton. E.A., Sáez.  
989 A.E., 2012. A review on the importance of metals and metalloids in atmospheric dust  
990 and aerosol from mining operations. *Science of the Total Environment* 433. 58-73.

991 de Blas, M. A. 1996. *La primera minería metálica del N. Peninsular: las*  
992 *indicaciones del C-14 y la cronología prehistórica de las explotaciones del Aramo y el*  
993 *Milagro. Complutum extra*, 217-266.

994 de Blas. M.A., 2005. *Un témoignage probant de l'exploitation préhistorique du*  
995 *cuivre dans le nord de la péninsule ibérique: le complexe minier de l'Aramo. Mém. S.*  
996 *Préhist. F.37. 195–205*

997 Dee. D.P., Uppala. S., Simmons. A., Berrisford. P., Poli. P., Kobayashi. S.,  
998 Andrae. U., Balmaseda. M., Balsamo. G., Bauer. d.P., 2011. *The ERA-Interim*  
999 *reanalysis: Configuration and performance of the data assimilation system. Quarterly*  
1000 *Journal of the royal meteorological society* 137. 553-597.

1001 Díez. E.G., Corella. J.P., Adatte. T., Thevenon. F., Loizeau. J.-L., 2017. *High-*  
1002 *resolution reconstruction of the 20th century history of trace metals, major elements,*  
1003 *and organic matter in sediments in a contaminated area of Lake Geneva, Switzerland.*  
1004 *Applied Geochemistry* 78. 1-11.

1005 Draxler. R.R., Stunder. B., Rolph. G., Taylor. J., 2009. *NOAA Air Resources*  
1006 *Laboratory. Silver Spring, MD. December 1997. revised January 2009.*  
1007 [http://www.arl.noaa.gov/documents/reports/hysplit\\_user\\_guide.pdf](http://www.arl.noaa.gov/documents/reports/hysplit_user_guide.pdf).

1008 Elbaz-Poulichet. F., Dezileau. L., Freydier. R., Cossa. D., Sabatier. P., 2011. *A*  
1009 *3500-year record of Hg and Pb contamination in a Mediterranean sedimentary archive*

1010 *(The Pierre Blanche Lagoon, France). Environmental Science & Technology* 45. 8642-  
1011 8647.

1012 *Elbaz-Poulichet. F., Guédron. S., Anne-Lise. D., Freydier. R., Perrot. V., Rossi.*  
1013 *M., Piot. C., Delpoux. S., Sabatier. P., 2020. A 10.000-year record of trace metal and*  
1014 *metalloid (Cu, Hg, Sb, Pb) deposition in a western Alpine lake (Lake Robert, France):*  
1015 *Deciphering local and regional mining contamination. Quaternary Science Reviews*  
1016 *228. 106076.*

1017 *EMEP. European Monitoring and Evaluation Programme <http://emep.int>.*

1018 *Enrico. M., Le Roux. G., Heimbürger. L.-E., Van Beek. P., Souhaut. M., Chmeleff.*  
1019 *J.r., Sonke. J.E., 2017. Holocene atmospheric mercury levels reconstructed from peat*  
1020 *bog mercury stable isotopes. Environmental Science & Technology* 51. 5899-5906.

1021 *Fain. X., Ferrari. C.P., Dommergue. A., Albert. M.R., Battle. M., Severinghaus.*  
1022 *J., Arnaud. L., Barnola. J.-M., Cairns. W., Barbante. C., 2009. Polar firn air reveals*  
1023 *large-scale impact of anthropogenic mercury emissions during the 1970s. Proceedings*  
1024 *of the National Academy of Sciences* 106. 16114-16119.

1025 *Fanlo. I., Touray. C.J., Subías. I., Fernández-Nieto. C., 1998. Geochemical*  
1026 *patterns of a sheared fluorite vein, Parzan, Spanish Central Pyrenees. Mineralium*  
1027 *Deposita* 33. 620-632.

1028 *Gallego. J.L., Ortiz. J.E., Sánchez-Palencia. Y., Baragaño. D., Borrego. Á.G.,*  
1029 *Torres. T., 2019. A multivariate examination of the timing and accumulation of*  
1030 *potentially toxic elements at Las Conchas bog (NW Spain). Environmental Pollution*  
1031 *254. 113048.*

1032 *García-Alix. A., Jiménez-Espejo. F.J., Lozano. J.A., Jiménez-Moreno. G.,*  
1033 *Martínez-Ruiz. F., Sanjuán. L.G., Jiménez. G.A., Alfonso. E.G., Ruiz-Puertas. G.,*

1034 *Anderson. R.S.. 2013. Anthropogenic impact and lead pollution throughout the*  
1035 *Holocene in Southern Iberia. Science of the Total Environment 449. 451-460.*

1036 *García-Ruiz. J.M.. López-Moreno. J.I.. Lasanta. T.. Vicente-Serrano. S.M..*  
1037 *González-Sampériz. P.. Valero-Garcés. B.L.. Sanjuán. Y.. Beguería. S.. Nadal-Romero.*  
1038 *E.. Lana-Renault. N.. 2015. Geo-ecological effects of Global Change in the Central*  
1039 *Spanish Pyrenees: A review at different spatial and temporal scales. Pirineos 170. e012.*

1040 *García-Ruiz. J.M.. Palacios. D.. de Andrés. N.. Valero-Garcés. B.L.. López-*  
1041 *Moreno. J.I.. Sanjuán. Y.. 2014. Holocene and 'little ice age' glacial activity in the*  
1042 *Marboré cirque. Monte Perdido Massif. Central Spanish Pyrenees. The Holocene 24.*  
1043 *1439-1452.*

1044 *George. L.L.. Cook. N.J.. Crowe. B.B.. Ciobanu. C.L.. 2018. Trace elements in*  
1045 *hydrothermal chalcopyrite. Mineralogical Magazine 82. 59-88.*

1046 *Girard. J.. Munoz. M.. Cauuet. B.. Polve. M.. Aries. S.. Callegarin. L.. 2010.*  
1047 *Silver Mines on the Massif of Montaignu (Hautes-Pyrénées. France): An Aquitanian*  
1048 *Network for Silver? Study on Lead Isotopes. ArchéoSciences. 235-242.*

1049 *Goldwater. L.J.. 1972. Mercury: a history of quicksilver. Baltimore: York Press*

1050 *González-Sampériz. P.. Aranbarri. J.. Pérez-Sanz. A.. Gil-Romera. G.. Moreno.*  
1051 *A.. Leunda. M.. Sevilla-Callejo. M.. Corella. J.P.. Morellón. M.. Oliva. B.. 2017.*  
1052 *Environmental and climate change in the southern Central Pyrenees since the Last*  
1053 *Glacial Maximum: A view from the lake records. Catena 149. 668-688.*

1054 *González-Sampériz. P.. Montes. L.. Aranbarri. J.. Leunda. M.. Domingo. R..*  
1055 *Laborda. R.. Sanjuan. Y.. Gil-Romera. G.. Lasanta. T.. García-Ruiz. J.. 2019. Scenarios.*  
1056 *timing and paleo-environmental indicators for the identification of Anthropocene in the*  
1057 *vegetal landscape of the Central Pyrenees (NE Iberia). Cuadernos de Investigación*  
1058 *Geográfica 45. 167-193.*

1059           Guyard. H.. Chapron. E.. St-Onge. G.. Anselmetti. F.S.. Arnaud. F.. Magand. O..  
1060   *Francus. P. Mélières. M.-A.. 2007. High-altitude varve records of abrupt environmental*  
1061   *changes and mining activity over the last 4000 years in the Western French Alps (Lake*  
1062   *Bramant. Grandes Rousses Massif). quaternary science reviews 26. 2644-2660.*

1063           Hamilton-Taylor. J.. Davison. W.. 1995. *Redox-driven cycling of trace elements*  
1064   *in lakes. Physics and chemistry of lakes. Springer. pp. 217-263.*

1065           Hanebuth. T.J.. King. M.L.. Mendes. I.. Lebreiro. S.. Lobo. F.J.. Oberle. F.K..  
1066   *Antón. L.. Ferreira. P.A.. Reguera. M.I.. 2018. Hazard potential of widespread but*  
1067   *hidden historic offshore heavy metal (Pb, Zn) contamination (Gulf of Cadiz, Spain).*  
1068   *Science of the Total Environment 637. 561-576.*

1069           Hansson. S.V.. Claustres. A.. Probst. A.. De Vleeschouwer. F.. Baron. S.. Galop.  
1070   *D.. Mazier. F.. Le Roux. G.. 2017. Atmospheric and terrigenous metal accumulation*  
1071   *over 3000 years in a French mountain catchment: Local vs distal influences.*  
1072   *Anthropocene 19. 45-54.*

1073           Hansson. S.V.. Grusson. Y.. Chimienti. M.. Claustres. A.. Jean. S.. Le Roux. G..  
1074   *2019. Legacy Pb pollution in the contemporary environment and its potential*  
1075   *bioavailability in three mountain catchments. Science of the Total Environment 671.*  
1076   *1227-1236.*

1077           Hernández. A. 2007. *Los mineros del azogue. Fundación Almadén 'Francisco*  
1078   *Javier de Villegas'. Almaden.*

1079           Hillman. A.L.. Abbott. M.B.. Valero-Garcés. B.. Morellon. M.. Barreiro-Lostres.  
1080   *F.. Bain. D.J.. 2017. Lead pollution resulting from Roman gold extraction in*  
1081   *northwestern Spain. The Holocene 27. 1465-1474.*

1082            *Hong. S., Candelone. J.-P., Patterson. C.C., Boutron. C.F., 1994. Greenland ice*  
1083 *evidence of hemispheric lead pollution two millennia ago by Greek and Roman*  
1084 *civilizations. Science 265. 1841-1843.*

1085            *Hong. S., Candelone. J.-P., Patterson. C.C., Boutron. C.F., 1996. History of*  
1086 *ancient copper smelting pollution during Roman and medieval times recorded in*  
1087 *Greenland ice. Science 272. 246-249.*

1088            *Horowitz. H.M., Jacob. D.J., Zhang. Y., Dibble. T.S., Slemr. F., Amos. H.M.,*  
1089 *Schmidt. J.A., Corbitt. E.S., Marais. E.A., Sunderland. E.M., 2017. A new mechanism*  
1090 *for atmospheric mercury redox chemistry: implications for the global mercury budget.*  
1091 *Atmospheric Chemistry and Physics 17. 6353-6371.*

1092            *Hylander. L.D., Meili. M., 2003. 500 years of mercury production: global annual*  
1093 *inventory by region until 2000 and associated emissions. Science of the Total*  
1094 *Environment 304. 13-27.*

1095            *Irabien. M.J., Cearreta. A., Urteaga. M., 2012. Historical signature of Roman*  
1096 *mining activities in the Bidasoa estuary (Basque Country, northern Spain): an*  
1097 *integrated micropalaeontological, geochemical and archaeological approach. Journal*  
1098 *of Archaeological Science 39. 2361-2370.*

1099            *Killick. D., Fenn. T., 2012. Archaeometallurgy: the study of preindustrial mining*  
1100 *and metallurgy. Annual Review of Anthropology 41.*

1101            *Komárek. M., Ettler. V., Chrástný. V., Mihaljevič. M., 2008. Lead isotopes in*  
1102 *environmental sciences: a review. Environment International 34. 562-577.*

1103            *Kylander. M.E., Weiss. D.J., Cortizas. A.M., Spiro. B., Garcia-Sanchez. R.,*  
1104 *Coles. B., 2005. Refining the pre-industrial atmospheric Pb isotope evolution curve in*  
1105 *Europe using an 8000 year old peat core from NW Spain. Earth and Planetary Science*  
1106 *Letters 240. 467-485.*

1107 Lavilla. I., Filgueiras. A., Valverde. F., Millos. J., Palanca. A., Bendicho. C.,  
1108 2006. Depth profile of trace elements in a sediment core of a high-altitude lake deposit  
1109 at the Pyrenees, Spain. *Water, air, and soil pollution* 172, 273-293.

1110 Le Roux. G., Fagel. N., De Vleeschouwer. F., Krachler. M., Debaille. V., Stille. P.,  
1111 Mattielli. N., Van Der Knaap. W.O., Van Leeuwen. J.F., Shotyk. W., 2012. Volcano-and  
1112 climate-driven changes in atmospheric dust sources and fluxes since the Late Glacial in  
1113 Central Europe. *Geology* 40, 335-338.

1114 Le Roux. G., Hansson. S.V., Claustres. A., Binet. S., De Vleeschouwer. F.,  
1115 Gandois. L., Mazier. F., Simonneau. A., Teisserenc. R., Allen. D., 2019. Trace Metal  
1116 Legacy in Mountain Environments. *Biogeochemical Cycles*, 191-206.

1117 Leblanc. M., Morales. J., Borrego. J., Elbaz-Poulichet. F., 2000. 4,500-year-old  
1118 mining pollution in southwestern Spain: long-term implications for modern mining  
1119 pollution. *Economic Geology* 95, 655-662.

1120 Leunda. M., Gil-Romera. G., Daniau. A.-L., Benito. B.M., González-Sampériz.  
1121 P., 2020. Holocene fire and vegetation dynamics in the Central Pyrenees (Spain).  
1122 *Catena* 188, 104411.

1123 Leunda. M., González-Sampériz. P., Gil-Romera. G., Aranbarri. J., Moreno. A.,  
1124 Oliva-Urcia. B., Sevilla-Callejo. M., Valero-Garcés. B., 2017. The Late-Glacial and  
1125 Holocene Marboré Lake sequence (2612 m asl, Central Pyrenees, Spain): testing high  
1126 altitude sites sensitivity to millennial scale vegetation and climate variability. *Global  
1127 and planetary change* 157, 214-231.

1128 López-Costas. O., Kylander. M., Mattielli. N., Álvarez-Fernández. N., Pérez-  
1129 Rodríguez. M., Mighall. T., Bindler. R., Cortizas. A.M., 2020. Human bones tell the  
1130 story of atmospheric mercury and lead exposure at the edge of Roman World. *Science of  
1131 the Total Environment* 710, 136319.

1132 *MacDonald. D.D., Ingersoll. C.G., Berger. T.A., 2000. Development and*  
1133 *evaluation of consensus-based sediment quality guidelines for freshwater ecosystems.*  
1134 *Arch. Environ. Contam. Toxicol. 39. 20-31.*

1135 *Manteca. J.-I., Ros-Sala. M., Ramallo-Asensio. S., Navarro-Hervás. F.,*  
1136 *Rodríguez-Estrella. T., Cerezo-Andreo. F., Ortiz-Menéndez. J.-E., de-Torres. T.,*  
1137 *Martínez-Andreu. M., 2017. Early metal pollution in southwestern Europe: the former*  
1138 *littoral lagoon of El Almarjal (Cartagena mining district, SE Spain). A sedimentary*  
1139 *archive more than 8000 years old. Environmental Science and Pollution Research 24.*  
1140 *10584-10603.*

1141 *Mariet. A.-L., Monna. F., Gimbert. F., Bégeot. C., Cloquet. C., Belle. S., Millet.*  
1142 *L., Rius. D., Walter-Simonnet. A.-V., 2018. Tracking past mining activity using trace*  
1143 *metals, lead isotopes and compositional data analysis of a sediment core from*  
1144 *Longemer Lake, Vosges Mountains, France. Journal of Paleolimnology 60. 399-412.*

1145 *Martín-Puertas. C., Martínez-Ruiz. F., Jimenez Espejo. F.J., Nieto-Moreno. V.,*  
1146 *Rodrigo. M., Mata. M.P., Valero-Garcés. B.L., 2010. Late Holocene climate variability*  
1147 *in the southwestern Mediterranean region: an integrated marine and terrestrial*  
1148 *geochemical approach. Climate of the Past 6. 807-816.*

1149 *Martínez-Cortizas. A., Pontevedra-Pombal. X., Munoz. J.N., García-Rodeja. E.,*  
1150 *1997. Four thousand years of atmospheric Pb, Cd and Zn deposition recorded by the*  
1151 *ombrotrophic peat bog of Penido Vello (Northwestern Spain). Water, air, and soil*  
1152 *pollution 100. 387-403.*

1153 *Martínez-Cortizas. A., Pontevedra-Pombal. X., García-Rodeja. E., Nóvoa. M., J.*  
1154 *C., Shotyk. W., 1999. Mercury in a Spanish Peat Bog: Archive of Climate Change and*  
1155 *Atmospheric Metal Deposition. Science 284. 939-942.*



1156 *Martínez-Cortizas. A., Garcia-Rodeja. E., Pombal X., P., Munoz JC., N., D., W.,*  
1157 *AK. C., 2002. Atmospheric Pb deposition in Spain during the last 4600 years recorded*  
1158 *by two ombrotrophic peat bogs and implications for the use of peat as archive. Science*  
1159 *of the Total Environment 292. 33-44.*

1160 *Martínez Cortizas. A., Peiteado Varela. E., Bindler. R., Biester. H., Cheburkin.*  
1161 *A., 2012. Reconstructing historical Pb and Hg pollution in NW Spain using multiple*  
1162 *cores from the Chao de Lamoso bog (Xistral Mountains). Geochimica et Cosmochimica*  
1163 *Acta 82. 68-78.*

1164 *Martínez-Cortizas. A., López-Merino. L., Bindler. R., Mighall. T., Kylander. M.,*  
1165 *2013. Atmospheric Pb pollution in N Iberia during the late Iron Age/Roman times*  
1166 *reconstructed using the high-resolution record of La Molina mire (Asturias, Spain).*  
1167 *Journal of Paleolimnology 50. 71-86.*

1168 *Martínez-Cortizas. A., López-Merino. L., Bindler. R., Mighall. T., Kylander.*  
1169 *M.E., 2016. Early atmospheric metal pollution provides evidence for*  
1170 *Chalcolithic/Bronze Age mining and metallurgy in Southwestern Europe. Science of the*  
1171 *Total Environment 545. 398-406.*

1172 *Martínez Cortizas. A., López-Costas. O., Orme. L., Mighall. T., Kylander. M.E.,*  
1173 *Bindler. R., Gallego Sala. A., 2020. Holocene atmospheric dust deposition in NW Spain.*  
1174 *The Holocene 30. 507-518.*

1175 *Martinon-Torres. M., Rehren. T., 2011. Mining. Europe. Encyclopedia of*  
1176 *Society and Culture in the Medieval World. Schlager. Dallas.*

1177 *McConnell. J.R., Chellman. N.J., Wilson. A.I., Stohl. A., Arienzo. M.M.,*  
1178 *Eckhardt. S., Fritzsche. D., Kipfstuhl. S., Opel. T., Place. P.F., Steffensen. J.P., 2019.*  
1179 *Pervasive Arctic lead pollution suggests substantial growth in medieval silver*

1180 *production modulated by plague, climate, and conflict. Proceedings of the National*  
1181 *Academy of Sciences 116. 14910-14915.*

1182 *McConnell. J.R., Wilson. A.I., Stohl. A., Arienzo. M.M., Chellman. N.J.,*  
1183 *Eckhardt. S., Thompson. E.M., Pollard. A.M., Steffensen. J.P., 2018. Lead pollution*  
1184 *recorded in Greenland ice indicates European emissions tracked plagues, wars, and*  
1185 *imperial expansion during antiquity. Proceedings of the National Academy of Sciences*  
1186 *115. 5726-5731.*

1187 *Mil-Homens. M., Vale. C., Brito. P., Naughton. F., Drago. T., Raimundo. J.,*  
1188 *Anes. B., Schmidt. S., Caetano. M., 2017. Insights of Pb isotopic signature into the*  
1189 *historical evolution and sources of Pb contamination in a sediment core of the*  
1190 *southwestern Iberian Atlantic shelf. Science of the Total Environment 586. 473-484.*

1191 *Montero-Ruiz. I., Castanyer. P., Gener. M., Hunt. M., Mata. J., Pons. H., Rovira-*  
1192 *Llorens. S., Rovira-Hortala. C., Renzi. M., Santos-Retolaza. M., 2007. Lead and silver*  
1193 *metallurgy in Emporion (L'Escala, Girona, Spain). Proceedings of the 2nd*  
1194 *International Conference on Archeometallurgy in Europe. Aquileia, Italy.*

1195 *More. A.F., Spaulding. N.E., Bohleber. P., Handley. M.J., Hoffmann. H.,*  
1196 *Korotkikh. E.V., Kurbatov. A.V., Loveluck. C.P., Sneed. S.B., McCormick. M., 2017.*  
1197 *Next-generation ice core technology reveals true minimum natural levels of lead (Pb) in*  
1198 *the atmosphere: Insights from the Black Death. GeoHealth 1. 211-219.*

1199 *Morellón. M., Pérez-Sanz. A., Corella. J.P., Büntgen. U., Catalán. J., González-*  
1200 *Sampériz. P., González-Trueba. J.J., López-Sáez. J.A., Moreno. A., Pla-Rabes. S., Saz-*  
1201 *Sánchez. M.A., Scussolini. P., Serrano. E., Steinhilber. F., Stefanova. V., Vegas-*  
1202 *Vilarrúbia. T., Valero-Garcés. B., 2012. A multi-proxy perspective on millennium-long*  
1203 *climate variability in the Southern Pyrenees. Climate of the Past 8. 683-700.*

- 1204 Moreno. A., Pérez. A., Frigola. J., Nieto-Moreno. V., Rodrigo-Gámiz. M.,  
1205 Martrat. B., González-Sampérez. P., Morellón. M., Martín-Puertas. C., Corella. J.P.,  
1206 Belmonte. Á., Sancho. C., Cacho. I., Herrera. G., Canals. M., Grimalt. J.O., Jiménez-  
1207 Espejo. F., Martínez-Ruiz. F., Vegas-Vilarrúbia. T., Valero-Garcés. B.L., 2012. *The*  
1208 *Medieval Climate Anomaly in the Iberian Peninsula reconstructed from marine and lake*  
1209 *records. Quaternary Science Reviews* 43. 16-32.
- 1210 Nicolás-Martínez. P.M., 2013. *Morfología del circo de Tucarroya (Macizo de*  
1211 *Monte Perdido, Pirineo aragonés). Cuadernos de Investigación Geográfica* 7. 51-80.
- 1212 Nieto-Callen. J.J., 1996. *El proceso sidero-metalúrgico altoaragones: Los valles*  
1213 *de Bielsa y Gistain en la Edad Moderna (1565-1800). Lull* 19. 471-507.
- 1214 Oliva. M., Ruiz-Fernández. J., Barriendos. M., Benito. G., Cuadrat. J.M.,  
1215 Domínguez-Castro. F., García-Ruiz. J.M., Giralt. S., Gómez-Ortiz. A., Hernández. A.,  
1216 López-Costas. O., López-Moreno. J.I., López-Sáez. J.A., Martínez-Cortizas. A., Moreno.  
1217 A., Prohom. M., Saz. M.A., Serrano. E., Tejedor. E., Trigo. R., Valero-Garcés. B.,  
1218 Vicente-Serrano. S.M., 2018. *The Little Ice Age in Iberian mountains. Earth-Science*  
1219 *Reviews* 177. 175-208.
- 1220 Oliva-Urcia. B., Moreno. A., Leunda. M., Valero-Garcés. B., González-Sampérez.  
1221 P., Gil-Romera. G., Mata. M., Group. H., 2018. *Last deglaciation and Holocene*  
1222 *environmental change at high altitude in the Pyrenees: the geochemical and*  
1223 *paleomagnetic record from Marboré Lake (N Spain). Journal of paleolimnology* 59.  
1224 349-371.
- 1225 Pèlachs. A., Nadal. J., Soriano. J.M., Molina. D., Cunill. R., 2009. *Changes in*  
1226 *Pyrenean woodlands as a result of the intensity of human exploitation: 2.000 years of*  
1227 *metallurgy in Vallferrera, northeast Iberian Peninsula. Vegetation History and*  
1228 *archaeobotany* 18. 403-416.

1229           Pérez. I.S.. González. I.F.. González. E.M.. SORIA. C.B.. 2008. *Explotaciones*  
1230 *mineras del entorno del Hospital de Benasque: geología y encuadre histórico. Macla:*  
1231 *revista de la Sociedad Española de Mineralogía. 239.*

1232           Pey. J.. Querol. X.. Alastuey. A.. Forastiere. F.. Stafoggia. M.. 2013. *African dust*  
1233 *outbreaks over the Mediterranean Basin during 2001-2011: PM10 concentrations.*  
1234 *phenomenology and trends. and its relation with synoptic and mesoscale meteorology.*  
1235 *Atmospheric Chemistry and Physics 13. 1395.*

1236           Pontevedra-Pombal. X.. Mighall. T.M.. Nóvoa-Muñoz. J.C.. Peiteado-Varela. E..  
1237 Rodríguez-Racedo. J.. García-Rodeja. E.. Martínez-Cortizas. A.. 2013. *Five thousand*  
1238 *years of atmospheric Ni. Zn. As. and Cd deposition recorded in bogs from NW Iberia:*  
1239 *prehistoric and historic anthropogenic contributions. Journal of Archaeological Science*  
1240 *40. 764-777.*

1241           Preunkert. S.. McConnell. J.R.. Hoffmann. H.. Legrand. M.. Wilson. A.I..  
1242 Eckhardt. S.. Stohl. A.. Chellman. N.J.. Arienzo. M.M.. Friedrich. R.. 2019. *Lead and*  
1243 *antimony in basal ice from Col du Dome (French Alps) dated with radiocarbon: A*  
1244 *record of pollution during antiquity. Geophysical Research Letters 46. 4953-4961.*

1245           Pujalte. V.. Robador. A.. Payros. A.. Samsó. J.M.. 2016. *A siliciclastic braid delta*  
1246 *within a lower Paleogene carbonate platform (Ordesa-Monte Perdido National Park.*  
1247 *southern Pyrenees. Spain): record of the Paleocene–Eocene thermal maximum*  
1248 *perturbation. Palaeogeography. palaeoclimatology. palaeoecology 459. 453-470.*

1249           Renberg. I.. Persson. M.W.. Emteryd. O.. 1994. *Pre-industrial atmospheric lead*  
1250 *contamination detected in Swedish lake sediments. Nature 368. 323-326.*

1251           Rodríguez. S.. Cuevas. E.. Prospero. J.. Alastuey. A.. Querol. X.. López-Solano.  
1252 J.. García. M.. Alonso-Pérez. S.. 2015. *Modulation of Saharan dust export by the North*  
1253 *African dipole. Atmospheric Chemistry and Physics 15. 7471.*

- 1254 *Pérez-Rodríguez. M., Biester. H., Aboal. J. R., Toro. M., Cortizas. A. M., 2019.*  
1255 *Thawing of snow and ice caused extraordinary high and fast mercury fluxes to lake*  
1256 *sediments in Antarctica. Geochimica et Cosmochimica Acta. 248. 109-122.*
- 1257 *Rosman. K.J., Chisholm. W., Hong. S., Candelone. J.-P., Boutron. C.F., 1997.*  
1258 *Lead from Carthaginian and Roman Spanish mines isotopically identified in Greenland*  
1259 *ice dated from 600 BC to 300 AD. Environmental Science & Technology 31. 3413-*  
1260 *3416.*
- 1261 *Rytuba. J.J., 2003. Mercury from mineral deposits and potential environmental*  
1262 *impact. Environmental Geology 43. 326-338.*
- 1263 *Salvador. P., Alonso-Pérez. S., Pey. J., Artíñano. B., Bustos. J.J.d., Alastuey. A.,*  
1264 *Querol. X., 2014. African dust outbreaks over the western Mediterranean Basin: 11-*  
1265 *year characterization of atmospheric circulation patterns and dust source areas.*  
1266 *Atmospheric Chemistry & Physics. 14. 6759–6775*
- 1267 *Samsó Escolá. J.M., Robador. A., 2018. Mapa geológico del Parque Nacional de*  
1268 *Ordesa y Monte Perdido. Escala 1:25.000. In: IGME (Ed.). Serie GeoNatur.*
- 1269 *Sánchez-España. J., Mata. M.P., Vegas. J., Morellón. M., Rodríguez. J.A.,*  
1270 *Salazar. Á., Yusta. I., 2018. Limnochemistry of the remote, high mountain Lake Marboré*  
1271 *(Ordesa and Monte Perdido National Park, Central Pyrenees): Stratification dynamics*  
1272 *and trace metal anomalies. Limnetica 37. 85-103.*
- 1273 *Sánchez-López. G., Hernández. A., Pla-Rabes. S., Toro. M., Granados. I., Sigrò.*  
1274 *J., Trigo. R.M., Rubio-Inglés. M., Camarero. L., Valero-Garcés. B., 2015. The effects of*  
1275 *the NAO on the ice phenology of Spanish alpine lakes. Climatic Change 130. 101-113.*
- 1276 *Sánchez-López. G., Hernández. A., Pla-Rabès. S., Trigo. R.M., Toro. M.,*  
1277 *Granados. I., Sáez. A., Masqué. P., Pueyo. J.J., Rubio-Inglés. M., 2016. Climate*  
1278 *reconstruction for the last two millennia in central Iberia: The role of East Atlantic*

1279 (EA). *North Atlantic Oscillation (NAO) and their interplay over the Iberian Peninsula.*  
1280 *Quaternary Science Reviews* 149. 135-150.

1281 Serrano. O., Mateo. M. A., Dueñas-Bohórquez. A., Renom. P., López-Sáez. J. A.,  
1282 Cortizas. A. M., 2011. *The Posidonia oceanica marine sedimentary record: A Holocene*  
1283 *archive of heavy metal pollution. Science of the Total Environment.* 409(22). 4831-4840.

1284 Serrano. O., Martínez-Cortizas. A., Mateo. M., Biester. H., Bindler. R., 2013.  
1285 *Millennial scale impact on the marine biogeochemical cycle of mercury from early*  
1286 *mining on the Iberian Peninsula. Global Biogeochemical Cycles* 27. 21-30.

1287 Stein, A.F., Draxler, R.R., Rolph, G.D., Stundt, B.J.B., M. D. Cohen. M.D., Ngan  
1288 F. 2015. *NOAA's HYSPLIT Atmospheric Transport and Dispersion Modeling System.*  
1289 *Bull. Amer. Meteor. Soc.* 96 (12): 2059–2077.

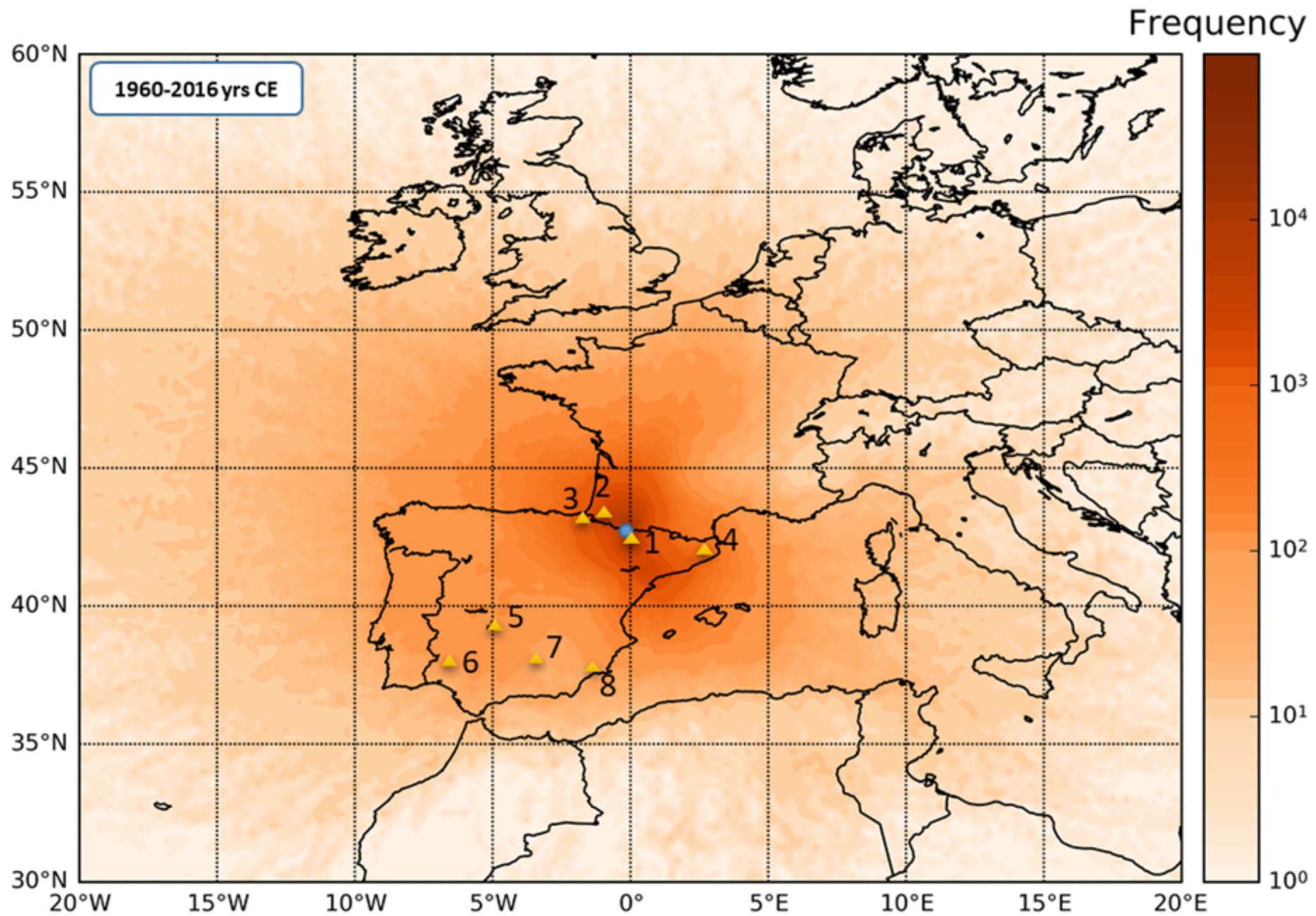
1290 Stos-Gale. Z.A., Gale. N.H., 2009. *Metal provenancing using isotopes and the*  
1291 *Oxford archaeological lead isotope database (OXALID). Archaeological and*  
1292 *Anthropological Sciences* 1. 195-213.

1293 Subías. I., Fanlo. I., Billström. K., 2015. *Ore-forming timing of polymetallic-*  
1294 *fluorite low temperature veins from Central Pyrenees: A Pb, Nd and Sr isotope*  
1295 *perspective. Ore Geology Reviews* 70. 241-251.

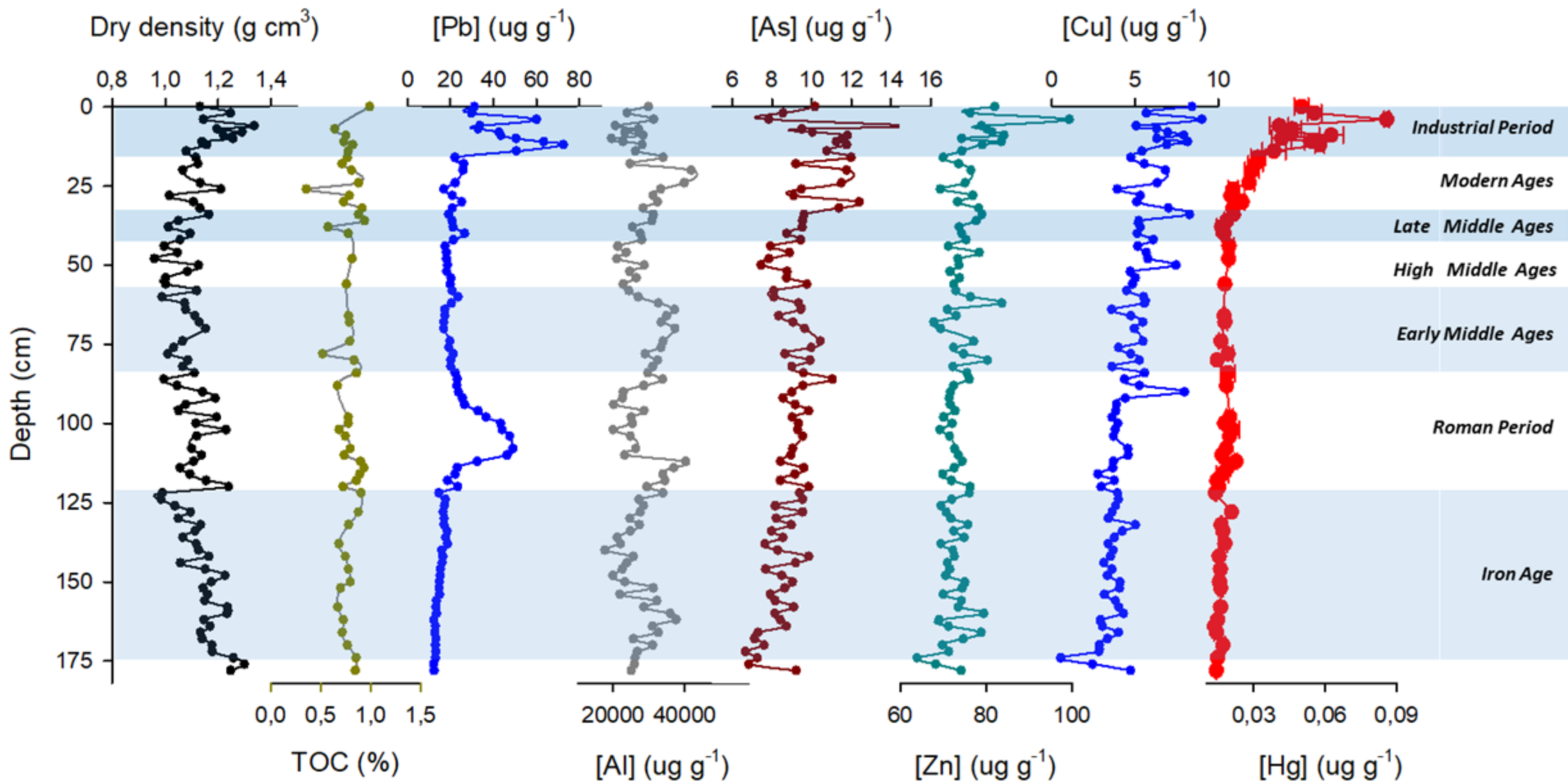
1296 Thalacker. J.G., 1804. *Noticias y descripción de las grandes explotaciones de*  
1297 *unas antiguas minas situadas al pie de los Pirineos y en la provincia de Guipúzcoa.*  
1298 *Variedades de Ciencias. Literatura y Artes* 4. 201-215.

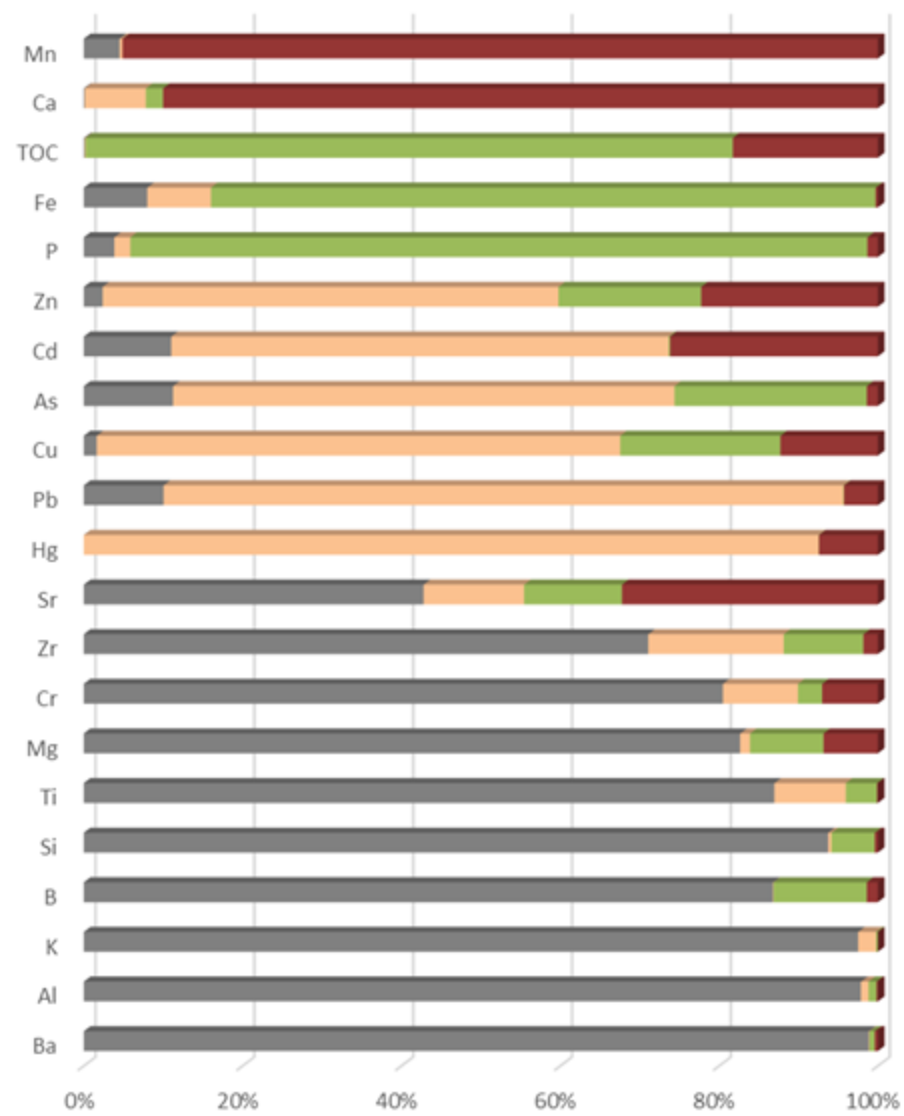
1299 Thevenon. F., Guédrón. S., Chiaradia. M., Loizeau. J.-L., Poté. J., 2011. (Pre-)  
1300 *historic changes in natural and anthropogenic heavy metals deposition inferred from*  
1301 *two contrasting Swiss Alpine lakes. Quaternary Science Reviews* 30. 224-233.

- 1302           Tylmann. W.. 2005. *Lithological and geochemical record of anthropogenic*  
1303 *changes in recent sediments of a small and shallow lake (Lake Pusty Staw, northern*  
1304 *Poland). Journal of Paleolimnology* 33. 313-325.
- 1305           Urteaga. M.. 2014. *Minería romana en el Cantábrico Oriental. Cuadernos de*  
1306 *Prehistoria y Arqueología de la Universidad de Granada* 24. 267-300.
- 1307           Valero-Garcés. B.L.. Oliva-Urcia. B.. Moreno Caballud. A.. Rico. M.T.. Mata-  
1308 *Campo. M.P.. Salazar-Rincón. A.. Rieradevall. M.. García-Ruiz. J.M.. Chueca Cía. J..*  
1309 *González-Sampériz. P.. 2013. Dinámica glacial. clima y vegetación en el Parque*  
1310 *Nacional de Ordesa y Monte Perdido durante el Holoceno. Proyectos de Investigación*  
1311 *en Parques Nacionales: 2009-2012 (MAGRAMA). 7-37*
- 1312           Velasco. F.. Pesquera. A.. Herrero. J.. 1996. *Lead isotope study of Zn-Pb ore*  
1313 *deposits associated with the Basque-Cantabrian basin and Paleozoic basement.*  
1314 *northern Spain. Mineralium Deposita* 31. 84-92.
- 1315           Vidal. R.. 2012. *La minería metálica prehistórica en la Península Ibérica.*  
1316 *Lurralde: invest. espac.* 35. 67-78.
- 1317           Weiss. D.. Shotyk. W.. Appleby. P.G.. Kramers. J.D.. Cheburkin. A.K.. 1999.  
1318 *Atmospheric Pb deposition since the industrial revolution recorded by five Swiss peat*  
1319 *profiles: enrichment factors. fluxes. isotopic composition. and sources. Environmental*  
1320 *Science & Technology* 33. 1340-1352.
- 1321           Wilhelm. B.. Vogel. H.. Anselmetti. F.. 2017. *A multi-centennial record of past*  
1322 *floods and earthquakes in Valle d'Aosta. Mediterranean Italian Alps. Natural Hazards*  
1323 *and Earth System Sciences* 17. 613-625.
- 1324           Wilson. A.. 2002. *Machines. power and the ancient economy. The Journal of*  
1325 *Roman Studies* 92. 1-32.

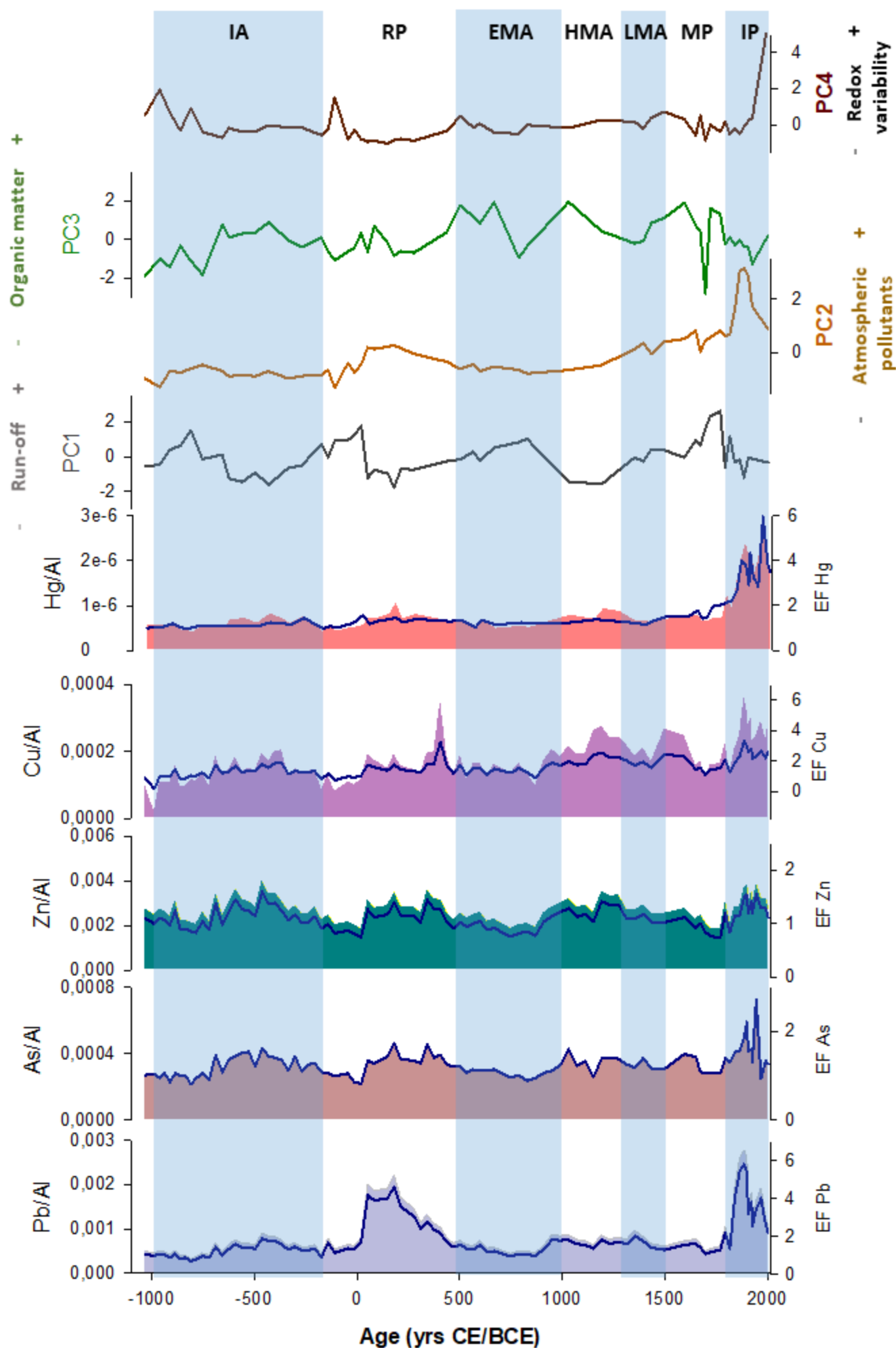


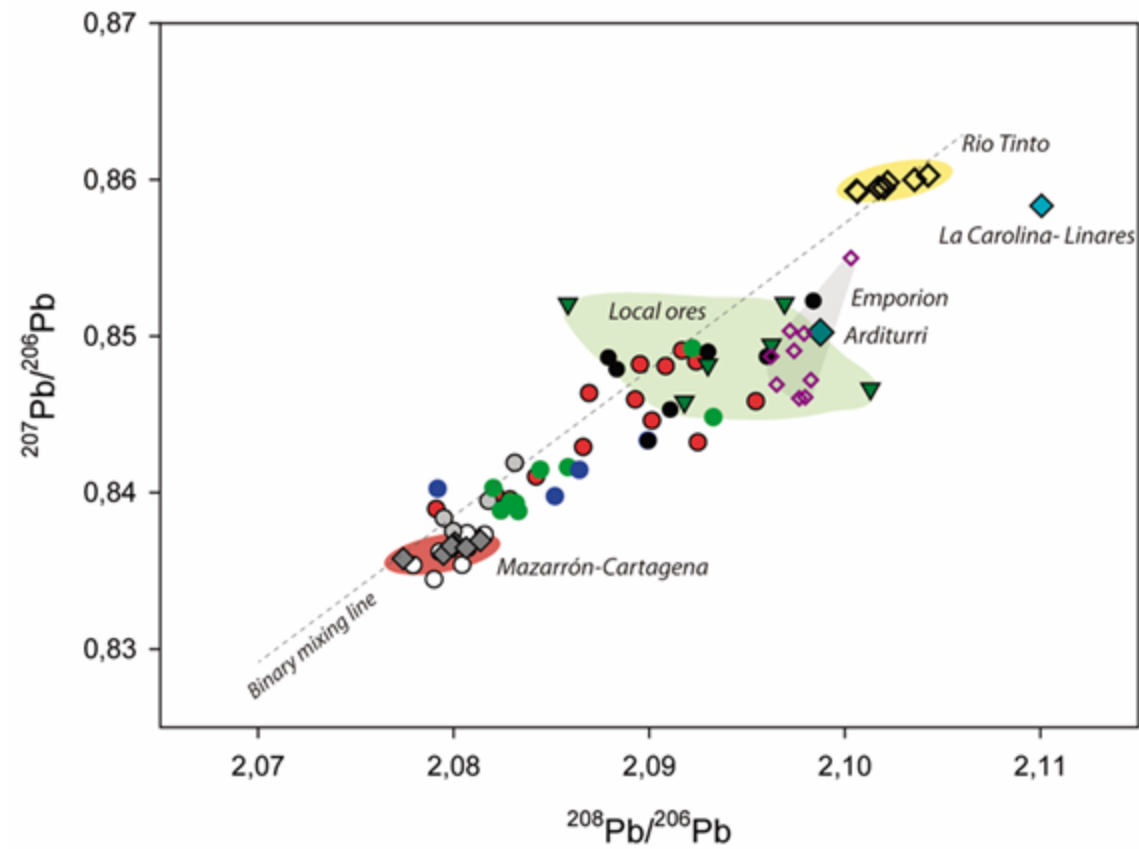






- PC1- Detrital input (watershed run-off)
- PC2- Atmospheric deposition of pollutants
- PC3- Organic deposition and nutrient input
- PC4- Lake's redox variability



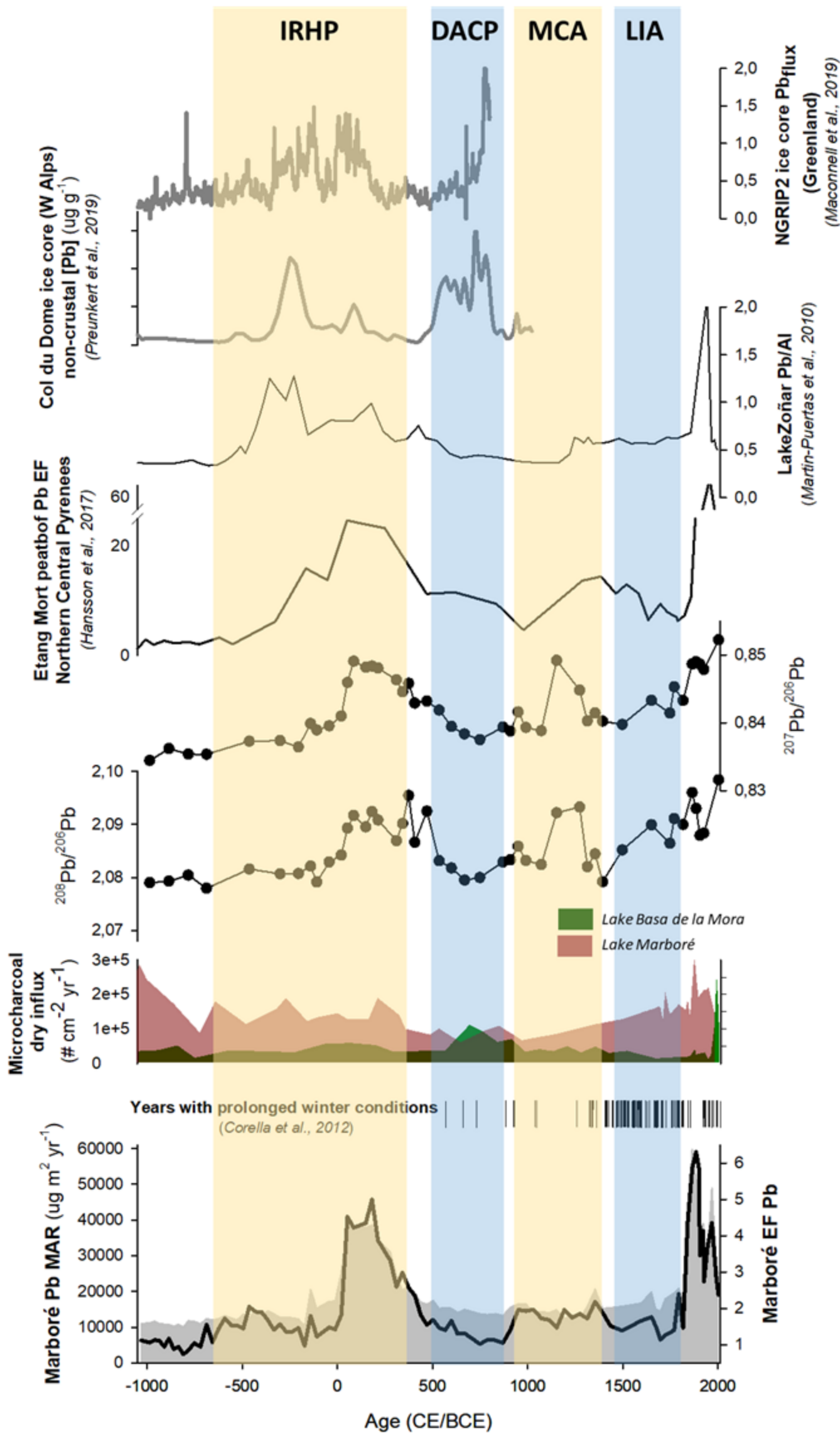


**Ore deposits from spanish mines**

- ◆ La Carolina - Linares
- ◇ Rio Tinto
- ◆ Mazarrón - Cartagena
- ◆ Arditurri
- ▼ Local ore deposits and small-scale mines in Central Pyrenees
- ◇ Emporion

**Lake Marbore**

- Late Iron/Iberian Period
- Roman Period
- Migration Period
- Middle Ages
- Modern Period
- Industrial Period



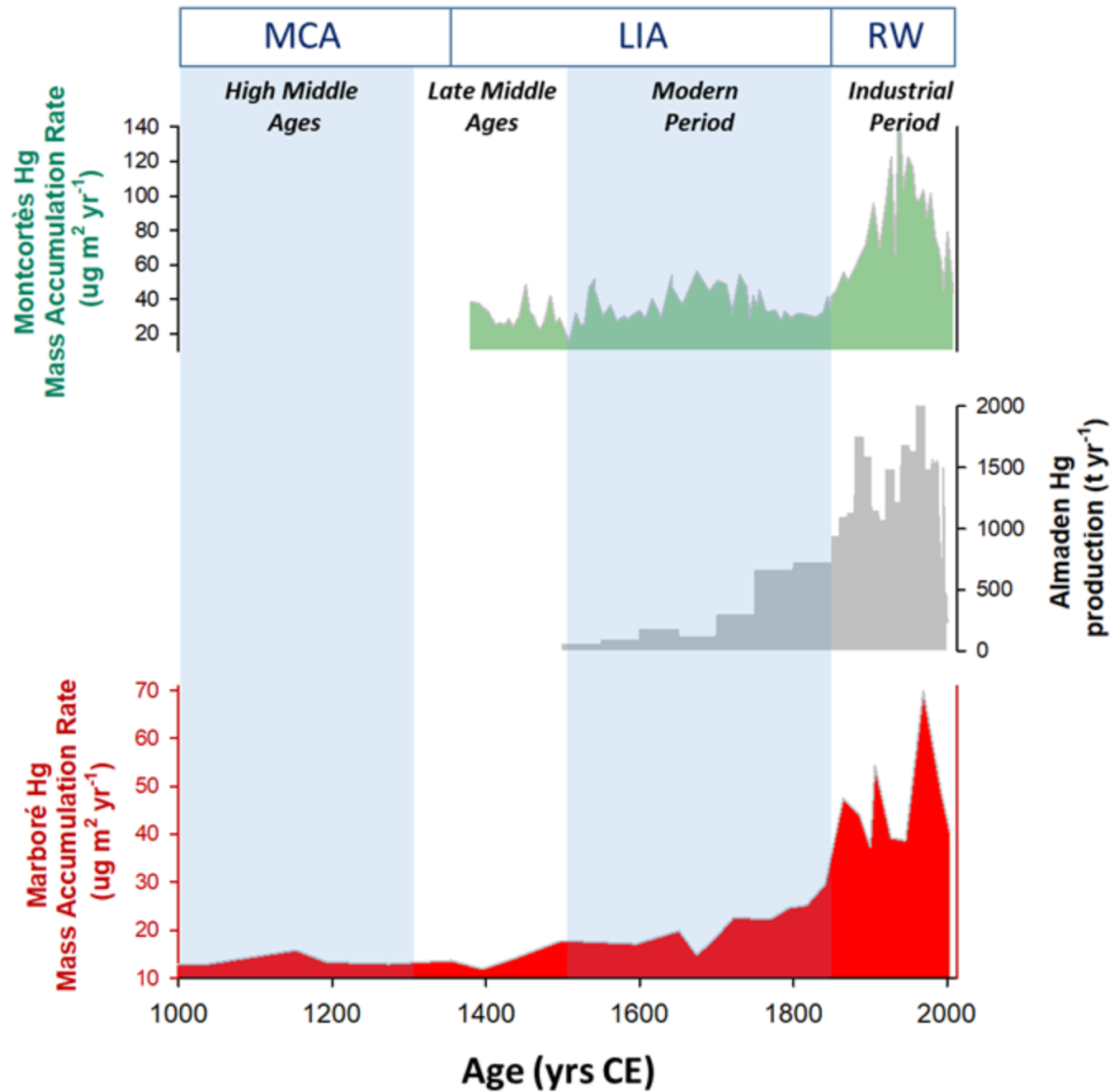


**Table 1:** Back trajectories percentages passing over different regions and arriving Lake Marboré area.

<b>Region</b>	<b>Longitude</b>	<b>Latitude</b>	<b>Percentage of back-trajectories /%</b>
SW France	42.83N - 45.83N	1.83W - 0.83E	51.9
Ebro valley	40.00N - 42.50E	1.83W - 2.83E	52.1
Central and western Spain	40.00N - 42.00N	10.00W - 2.5W	16.4
Southern Spain	36.00N - 40.00N	10.00W - 1.00E	17.4
Northern Africa	30.00N - 36.00N	10.00W - 5.00E	3.0

**Table 2:** Results of the Principal Component Analyses using the scores (loading factors) of the extracted principal components obtained for the geochemical datasets.

<b>Element</b>	<b>PC1</b>	<b>PC2</b>	<b>PC3</b>	<b>PC4</b>
Ba	0.98	-0.03	0.08	0.06
Al	0.97	-0.10	0.10	0.04
K	0.95	-0.14	0.04	0.01
B	0.91	0.03	0.33	0.12
Si	0.89	-0.06	-0.22	0.06
Ti	0.88	0.28	0.19	0.03
Mg	0.85	0.10	0.29	0.25
Cr	0.85	0.29	0.16	0.25
Zr	0.81	0.39	0.30	0.13
Sr	0.63	0.34	0.34	0.54
Hg	-0.01	0.90	-0.02	0.26
Pb	-0.26	0.77	-0.02	-0.17
Cu	0.12	0.73	0.41	0.32
As	0.30	0.71	0.44	-0.10
Cd	0.27	0.64	-0.03	0.41
Zn	0.12	0.59	0.33	0.37
P	0.18	0.13	0.88	-0.10
Fe	0.26	0.26	0.83	0.05
TOC	0.03	-0.02	0.72	0.34
Ca	0.03	0.25	0.13	0.85
Mn	0.15	0.04	0.00	0.68
<i>PCA variance</i>	<i>46.70</i>	<i>19.57</i>	<i>8.69</i>	<i>6.88</i>
<i>Accumulated variance</i>	<i>46.70</i>	<i>66.27</i>	<i>74.96</i>	<i>81.84</i>



# Reconstruction of the mining-related pollution legacy in high-altitude lacustrine ecosystems

